

# Not All Pairs are Equal: Hierarchical Learning for Average-Precision-Oriented Video Retrieval

Yang Liu  
SCST, UCAS  
liuyang232@mailsucas.ac.cn

Qianqian Xu\*  
IIP, ICT, CAS  
xuqianqian@ict.ac.cn

Peisong Wen  
IIP, ICT, CAS  
SCST, UCAS  
wenpeisong20z@ict.ac.cn

Siran Dai  
IIE, CAS  
SCS, UCAS  
daisiran@iie.ac.cn

Qingming Huang\*  
SCST, UCAS  
IIP, ICT, CAS  
BDKM, CAS  
Peng Cheng Laboratory  
qmhuang@ucas.ac.cn

## ABSTRACT

The rapid growth of online video resources has significantly promoted the development of video retrieval methods. As a standard evaluation metric for video retrieval, Average Precision (AP) assesses the overall rankings of relevant videos at the top list, making the predicted scores a reliable reference for the users. However, recent video retrieval methods utilize pair-wise losses that treat all sample pairs equally, leading to an evident gap between the training objective and evaluation metric. To effectively bridge this gap, in this work, we aim to address two primary challenges: **a)** The current similarity measure and AP-based loss are suboptimal for video retrieval; **b)** The noticeable noise from frame-to-frame matching introduces ambiguity in estimating the AP loss. In response to these challenges, we propose the *Hierarchical learning framework for Average-Precision-oriented Video Retrieval (HAP-VR)*. For the former challenge, we develop the TopK-Chamfer Similarity and QuadLinear-AP loss to measure and optimize video-level similarities in terms of AP. For the latter challenge, we suggest constraining the frame-level similarities to achieve an accurate AP loss estimation. Experimental results present that HAP-VR outperforms existing methods on several benchmark datasets, providing a feasible solution for video retrieval tasks and thus offering potential benefits for the multi-media application.

## CCS CONCEPTS

• **Information systems** → *Video search; Learning to rank.*

## KEYWORDS

Video Retrieval; Average Precision; Hierarchical Similarity Optimization; Self-supervised Learning

Permission to make digital or hard copies of all or part of this work for personal or classroom use is granted without fee provided that copies are not made or distributed for profit or commercial advantage and that copies bear this notice and the full citation on the first page. Copyrights for components of this work owned by others than the author(s) must be honored. Abstracting with credit is permitted. To copy otherwise, to publish, to post on servers or to redistribute to lists, requires prior specific permission and/or a fee. Request permissions from [permissions@acm.org](mailto:permissions@acm.org).  
MM '24, October 28–November 1, 2024, Melbourne, VIC, Australia.

© 2024 Copyright held by the owner/author(s). Publication rights licensed to ACM.  
ACM ISBN 979-8-4007-0686-8/24/10  
<https://doi.org/XXXXXXX.XXXXXXX>

## ACM Reference Format:

Yang Liu, Qianqian Xu, Peisong Wen, Siran Dai, and Qingming Huang. 2024. Not All Pairs are Equal: Hierarchical Learning for Average-Precision-Oriented Video Retrieval. In *Proceedings of the 32nd ACM International Conference on Multimedia (MM '24)*, October 28–November 1, 2024, Melbourne, VIC, Australia. *Proceedings of the 32nd ACM International Conference on Multimedia (MM'24)*, October 28–November 1, 2024, Melbourne, Australia. ACM, New York, NY, USA, 16 pages. <https://doi.org/XXXXXXX.XXXXXXX>

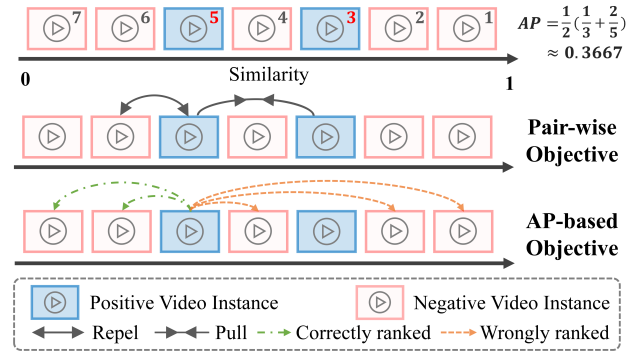


**Figure 1: Average Precision (AP) measures the average ranking of positive instances within a list, providing a comprehensive evaluation of the overall performance of the retrieval results. Pair-wise training objectives focus solely on pulling the positive instances closer while repelling the negative ones, failing to align with the AP metric. In contrast, AP-based objectives ensure this alignment by rectifying the rankings of mis-ranked positive-negative pairs in the list.**

## 1 INTRODUCTION

The rapid expansion of online video resources has made content-based video retrieval a crucial component for multi-media applications such as recommendation, video editing, and online education [1, 26]. As a fundamental task, video retrieval, aiming to efficiently and effectively rank candidate videos based on their

\*Corresponding authors.

similarities to the query video, has raised a wave of studies in the multi-media community.

Recent video retrieval methods [30, 32–34, 53] employ neural network models to learn video similarities by aggregating fine-grained embeddings of video frames, which have achieved a remarkable success compared with the early hand-craft approaches [11, 16, 28, 56, 59]. Nevertheless, **these models are typically optimized by pair-wise training objectives such as triplet loss, which are inconsistent with the evaluation metric.** Concretely, as a standard evaluation metric, Average Precision (AP) focuses on the top list by assigning larger weights to the top-ranked positive videos. Since the retrieval results are commonly processed sequentially in downstream tasks, the performance of the top list becomes crucial, thus making AP a more comprehensive metric as it better reflects this practical requirement. However, as shown in Figure 1, pair-wise losses treat all mis-ranked video pairs equally, ignoring the relative rankings among the instance list. This leads to an evident gap between the training objective and the evaluation metric, calling for an effective AP-based objective function to bridge this gap.

To solve a similar problem in image retrieval, a promising method is to optimize AP directly. Due to the non-differentiability of AP, existing methods focus on differential approximations for AP [4, 6, 7, 47, 49, 58, 63, 64]. Although these AP optimization methods have achieved notable success in the image field, they cannot be directly applied to videos due to the complexity arising from the additional temporal dimension. Generally, the challenges are two-fold:

**a) The current similarity measure and the surrogate AP loss are suboptimal for AP-oriented video retrieval.** Typically, in mainstream frameworks, image similarities are measured with the cosine similarity of an embedding pair, while video similarities are aggregated from the redundant temporal-spatial features. Since AP jointly considers the rankings of all instances rather than merely distinguishing whether a pair of videos matches, it is necessary to design a fine-grained similarity measure function for videos. Additionally, existing surrogate AP losses like Smooth-AP [4] suffer from a vanishing gradient when a sample pair is seriously mis-ranked, leading to inefficient optimization. This phenomenon is more obvious for videos since the various video similarities fall into the gradient vanishing area more frequently.

**b) The noisy frame-to-frame matching leads to a biased AP estimation.** As illustrated in Figure 2, two relevant videos may not exhibit uniform relevance across all frames. Without fine-grained annotations, this ambiguity leads to false positive matching [65]. In this case, the weights of the top-ranked videos might be reduced, hindering the AP loss from concentrating on the top list.

Based on the above considerations, we propose the *Hierarchical learning framework for Average-Precision-oriented Video Retrieval (HAP-VR)*, which contains video-level and frame-level constraints as detailed following.

To tackle challenge **a)**, we propose a topK-based similarity measure and a variant of AP loss with sufficient large gradients. As a core component of our framework, the proposed *TopK-Chamfer Similarity* aggregates video-level similarities from frame-level similarities. Compared with previous maximum/average aggregations, the TopK-Chamfer Similarity retains fine-grained information while filtering out false correlations, providing refined video similarity for the following AP loss estimation. Another core component is

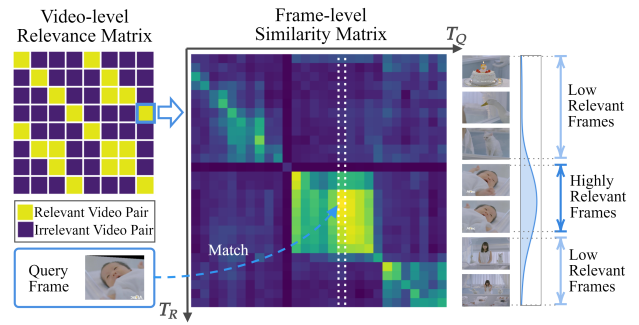


**Figure 2: Two relevant videos might not exhibit consistent relevance across all frame pairs due to the obvious redundancy and noise in the temporal dimension. Specifically, only a few consecutive frames in the candidate video are relevant to a given query frame.  $T_Q$  and  $T_R$  axes represent the time-lines of the query and reference videos, respectively.**

a new surrogate AP loss, namely *QuadLinear-AP*, which enjoys a more reasonable distribution of gradients to rectify mis-ranked positive-negative pairs efficiently.

In search of a solution to challenge **b)**, we propose to correct the frame-level similarities without requiring fine-grained annotations. Motivated by the recent advance in self-supervised learning [9, 21, 25], we leverage the pre-trained vision model [8] to extract frame-level representations. Subsequently, we generate pseudo labels indicating the matched frames from the gap between these representations and distill the frame-level information to avoid ambiguity, leading to a more precise estimation of AP loss.

To summarize, the contributions of this work are three-fold:

- We develop a self-supervised hierarchical learning framework for Average-Precision-oriented video retrieval, named HAP-VR, to fill the gap between training objectives and evaluation metrics that the previous work has overlooked.
- Within HAP-VR, we propose the TopK-Chamfer Similarity and QuadLinear-AP loss to measure and optimize video-level similarities of the AP metric, alongside constraining frame-level similarities to produce a precise estimation of AP loss.
- Our experimental evaluation of HAP-VR across several large-scale benchmark datasets often presents a superior performance in terms of AP, ensuring its effectiveness for content-based video retrieval tasks.

## 2 RELATED WORK

In this section, we will introduce several previous works that contribute to video retrieval and Average Precision optimization.

### 2.1 Video Retrieval

Based on the granularity of similarity processing, video retrieval methods can be generally classified into two schemes, i.e. coarse-grained method and fine-grained method.

**2.1.1 Coarse-grained Method.** This kind of method focuses on extracting and aggregating features into a vector space, representing each video by a single vector to compute similarity at the video

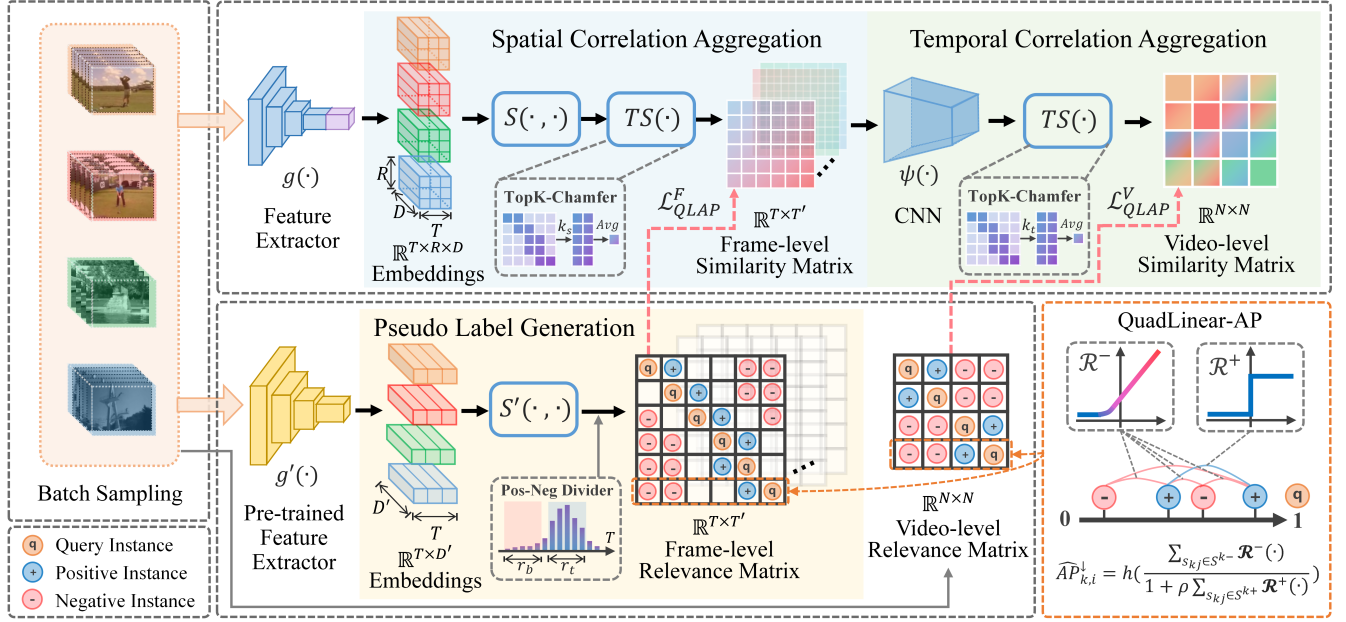


**Figure 3: The architecture of our proposed framework. The data batch is processed through a feature extractor to obtain patch-level embeddings. Afterward, we compute frame-level and video-level similarity matrices utilizing spatial and temporal correlation aggregation modules in sequence. Simultaneously, the batch is fed into a pre-trained self-supervised model to generate pseudo labels that indicate frame-level relevance. Ultimately, we apply the QuadLinear-AP to both the frame-level and video-level similarity matrices and backpropagate the loss to optimize the model’s parameters.**

level. In the early stage, methods such as Bag-of-Words [5, 51], code books [31, 37] encode videos into a single vector by summarizing the extracted features through statistical aggregation, which neglect the temporal and spatial structures of the video. With the advent of deep learning in the video field, later approaches have started to train deep neural networks with metric learning [32, 36], promoting the transition from coarse-grained methods to fine-grained methods in the subsequent research.

**2.1.2 Fine-grained Method.** This kind of method typically extracts features from frames and thus generates multiple vectors to represent a video. Early fine-grained methods focus on designing video temporal alignment solutions, e.g. temporal Hough Voting [16, 28], graph-based Temporal Network [56, 59] and Dynamic Programming [11], to match similar segments within the videos through hand-craft algorithms. Following the development of methods like TMK [46] and LAMV [2], which use Fourier transform and kernel tricks for spatio-temporal representation learning, there has been a shift towards transformer-based architectures [17, 23, 24, 46, 53]. Among these methods, TCA [53] adopts a self-attention mechanism to capture temporal relationships among fine-grained features and uses a contrastive learning strategy for training, VRL [24] combines CNN with a transformer structure to train a model without labels.

Recent methods concentrate on designing neural networks to learn similarity functions for calculating video-level similarities from original video representations. ViSiL [30] provides a supervised learning method that designs a CNN to obtain video-level similarities from frame-level similarities. Additionally, DnS [34]

employs knowledge distillation to train the student networks with ViSiL serving as a teacher network. More recently, S<sup>2</sup>VS [33] proposes a self-supervised learning approach based on an improved structure of ViSiL. Despite previous studies developing increasingly complex models, their reliance on training with pair-wise objectives has led to a misalignment with the evaluation metric. Furthermore, these efforts typically focus solely on optimizing video-level similarity, neglecting the importance of frame-level similarity learning. In our work, we propose a method that employs an AP-based objective to bridge this gap, hierarchically optimizing AP for both frame-level and video-level similarities during the learning process.

## 2.2 Average Precision Optimization

Traditional metric learning methods provide a learning paradigm for retrieval tasks, mapping instances into an embedding space and employing distance metrics to design pair-wise objective functions such as contrastive loss [10] or triplet loss [62]. However, these methods merely focus on increasing the distance between positive and negative instances within pairs or tuples, neglecting to improve the overall ranking of positives more comprehensively. This narrow focus can lead to overfitting, particularly in the face of imbalanced data distribution. A promising method is learning with ranking-based metrics as the target [60, 61, 66, 67], such as AP. However, the non-differentiability of ranking terms in AP poses a challenge, obstructing the update of model parameters during backpropagation. Numerous AP optimization methods have been developed to address this issue. Listwise approaches [6, 7, 47, 58] utilize differentiable histogram binning to optimize loss functions based on

ranking lists. Others provide structured learning frameworks based on SVM [40, 68] or conduct direct loss minimization [20, 54] to optimize AP. Moreover, BlackBox combinatorial solvers [45, 49] are proposed to differentiate the ranking terms in AP. More recently, Smooth-AP [4] introduces the Sigmoid function to approximate the indicator function, offering a simple and efficient way to differentiate AP. However, approximation methods like Smooth-AP neglect the gradient vanishing in the low AP area. To this end, we propose QuadLinear-AP, a novel loss for AP optimization, to designate appropriate gradients to the improperly ranked positive-negative pairs, ensuring the efficiency of the optimization process.

## 3 METHODOLOGY

### 3.1 Task Definition

In the video space  $\mathcal{X}$ , each video can be seen as a tensor  $\mathbf{V} = \{\mathbf{v}_j \in \mathbb{R}^{H \times W \times C}\}_{j=1}^T$  where  $T, H, W$ , and  $C$  represent the dimension of time, height, width, and channel, respectively. Given a pair of videos  $\mathbf{V}_1, \mathbf{V}_2 \in \mathcal{X}$ , video similarity learning aims to learn a similarity function  $f: \mathcal{X} \times \mathcal{X} \rightarrow \mathbb{R}$ , such that  $f(\mathbf{V}_1, \mathbf{V}_2)$  represents the relevance between  $\mathbf{V}_1, \mathbf{V}_2$ . During the training stage, at each step, we sample a batch of videos  $\mathbf{B} = \{\mathbf{V}_i \in \mathcal{X}\}_{i=1}^N$  where the length of  $\mathbf{V}_i$  is  $T_i$ . Let  $\mathbf{Y} \in \{0, 1\}^{N \times N}$  be the video-level relevance matrix, where  $Y_{ij} = 1$  if  $\mathbf{V}_i$  and  $\mathbf{V}_j$  are relevant or  $Y_{ij} = 0$  otherwise. For clarity, we denote the similarity score as  $s_{ij} = f(\mathbf{V}_i, \mathbf{V}_j)$ , and denote the rankings among positive/negative subsets as  $\mathcal{S}^{k+} = \{s_{ki} = f(\mathbf{V}_k, \mathbf{V}_i) | \mathbf{V}_i \in \mathbf{B}, Y_{ki} = 1, k \neq i\}$ ,  $\mathcal{S}^{k-} = \{s_{ki} = f(\mathbf{V}_k, \mathbf{V}_i) | \mathbf{V}_i \in \mathbf{B}, Y_{ki} = 0\}$ .

According to the above definition, we aim to optimize  $f$  such that  $f(\mathbf{V}_k, \mathbf{V}_i) > f(\mathbf{V}_k, \mathbf{V}_j)$  if  $Y_{ki} = 1$  and  $Y_{kj} = 0$ , such that it achieves a higher AP score:

$$\begin{aligned} \max_f AP(f) &= \frac{1}{N} \sum_{k=1}^N AP_k(f), \\ AP_k(f) &= \frac{1}{|\mathcal{S}^{k+}|} \sum_{s_{ki} \in \mathcal{S}^{k+}} \frac{\mathcal{R}(s_{ki}, \mathcal{S}^{k+})}{\mathcal{R}(s_{ki}, \mathcal{S}^{k+} \cup \mathcal{S}^{k-})}, \end{aligned} \quad (1)$$

where  $\mathcal{R}(s, \mathcal{S}) = 1 + \sum_{s' \in \mathcal{S}} \mathcal{H}(s' - s)$  is the descending ranking of  $s$  in  $\mathcal{S}$ ,  $\mathcal{H}(\cdot)$  is the Heaviside function [69], i.e.,  $\mathcal{H}(x) = 1$  if  $x > 0$  otherwise  $\mathcal{H}(x) = 0$ .

### 3.2 Overview

We aim to design an AP-oriented framework for video similarity learning to align the training objective with the evaluation metric of video retrieval. As illustrated in Figure 3, for two videos  $\mathbf{V}, \mathbf{V}' \in \mathcal{X}$  in a batch, we first utilize a feature extractor  $g(\cdot)$  to extract patch-level embeddings  $g(\mathbf{V}), g(\mathbf{V}') \in \mathbb{R}^{T \times R \times D}$ , where  $T, R, D$  are the number of frames, patches, and the embedding dimension, respectively. Afterward, the patch-to-patch similarities are measured with the cosine similarity, resulting in a patch-level similarity matrix  $S(\mathbf{V}, \mathbf{V}') \in \mathbb{R}^{T \times R \times R \times T'}$ .

Next, we optimize the similarity measure in a hierarchical strategy. At the video level, we aggregate the spatial and temporal correlation to video-level similarities via the proposed TopK-Chamfer Similarity (detailed in Section 3.3). Following ViSiL [30], we also apply a CNN to propagate the inter-frame similarities. Afterward,

the video-level similarities are input into the proposed QuadLinear-AP loss. As outlined in Section 3.4, for the frame-level constraint, we leverage a pre-trained vision model to generate pseudo labels and distill the frame-to-frame similarities to our feature extractor with the QuadLinear-AP loss.

### 3.3 Video-oriented AP Optimization

In this subsection, we first implement the similarity function  $f$  through a bottom-up video similarity measure to map patch-level embeddings into similarities. Following this, we propose an AP surrogate loss with appropriate gradients for optimization, instructing  $f$  to rank the similarities accurately.

**3.3.1 Bottom-up Video Similarity Measure.** In this subsection, we present the detailed process of feature aggregation. Specifically, given a pair of videos, we first aggregate the patch-level similarities  $S(\mathbf{V}, \mathbf{V}') \in \mathbb{R}^{T \times R \times R \times T'}$  along the spatial dimension, leading to a frame-level similarity matrix  $m_s(\mathbf{V}, \mathbf{V}') \in \mathbb{R}^{T \times T'}$ . Afterward, we aggregate the temporal dimension as the video-level similarity  $f(\mathbf{V}, \mathbf{V}') = m_t(\mathbf{V}, \mathbf{V}')$ . Consider a batch of videos  $\mathbf{B} = \{\mathbf{V}_i\}_{i=1}^N$ , similarities of all pairs form an  $N \times N$  video-level similarity matrix.

Early work utilizes a maximum/average operator to gather the fine-grained features. Kordopatis-Zilos *et al.* [30] suggest that two relevant frames/videos might be similar only in a part of region/period. From this perspective, to gather the spatial features, they propose to focus on the most similar region in  $g(\mathbf{V}')$  for each query patch in  $g(\mathbf{V})$ , leading to the Chamfer-Similarity-based aggregation [3]:

$$m_s(\mathbf{V}, \mathbf{V}')_{x,y} = \frac{1}{R} \sum_{j=1}^R \max_{i=1, \dots, R} S(\mathbf{V}, \mathbf{V}')_{x,i,j,y}. \quad (2)$$

The above operator identifies the maximum score for each query patch and averages these scores of all query patches in a frame to reflect the similarity between two frames. A similar operation is performed to gather the temporal features.

However, focusing on the maximum score makes the similarity measure sensitive to spatial noises caused by distractors. Besides, different from the patch-to-patch similarity matrix with a fixed shape, the temporal dimension in videos is flexible and varies greatly. Furthermore, given a query video  $\mathbf{V}_k$  and two relevant candidate videos  $\mathbf{V}_1, \mathbf{V}_2$ , the Chamfer Similarity might assign equal similarities for both  $\mathbf{V}_1$  and  $\mathbf{V}_2$ , even if  $\mathbf{V}_2$  contains more relevant frames. Such a phenomenon reduces the distinguishability of positive samples, leading to an ambiguous ranking estimation.

Therefore, we seek a fine-grained similarity measure to estimate a precise AP loss. Specifically, rather than taking the maximum value, we jointly consider the top K scores:

$$m_s(\mathbf{V}, \mathbf{V}')_{x,y} = \frac{1}{RK} \sum_{i=1}^R \sum_{j=1}^K S(\mathbf{V}, \mathbf{V}')_{x,i,[j],y}, \quad (3)$$

where  $K = k_s \times R$  and  $S(\mathbf{V}, \mathbf{V}')_{x,i,[j],y}$  refers to the  $j$ -th largest value, or formally:  $S(\mathbf{V}, \mathbf{V}')_{x,i,[1],y} \geq \dots \geq S(\mathbf{V}, \mathbf{V}')_{x,i,[R],y}$ .

On top of the frame-level similarities, following ViSiL [30], we utilize a CNN block  $\psi$  to fuse the frame-to-frame similarities:

$$\bar{m}_s(\mathbf{V}, \mathbf{V}') = \psi(m_s(\mathbf{V}, \mathbf{V}')) \in \mathbb{R}^{\frac{T}{s} \times \frac{T'}{s}}, \quad (4)$$

where  $s > 1$  is the downsampling factor of  $\psi$ . In this way, the frame-level similarity is mapped into a learnable measure space. Additionally, it downscales the similarity matrix to reduce the computational burden. Afterward, we utilize the proposed TopK-Chamfer Similarity in the temporal dimension, leading to the video-level similarity:

$$f(V, V') = m_t(V, V') = \frac{1}{T} \sum_{i=1}^T \sum_{j=1}^K \bar{m}_s(V, V')_{i,[j]}, \quad (5)$$

where  $K = k_t \times T'$  and  $\bar{m}_s(V, V')_{i,[1]} \geq \dots \geq \bar{m}_s(V, V')_{i,[T']}$ . On one hand, compared with the original Chamfer Similarity, the TopK-Chamfer Similarity maintains fine-grained information; on the other hand, compared with the average operator, it avoids the disturbing noise introduced by the irrelevant frames.

**3.3.2 Gradient-Enhanced AP Surrogate Loss.** To effectively update the fine-grained similarity measure, in this part, we propose a new surrogate AP loss, such that it enjoys proper gradients in the mis-ranked area.

For a batch of videos  $\mathcal{B} = \{V_i \in \mathcal{X}\}_{i=1}^N$ , recall that for a query video  $V_k$ , the similarity scores of the relevant and irrelevant videos are denoted as  $S^{k+} = \{s_{ki} = f(V_k, V_i) | V_i \in \mathcal{B}, Y_{ki} = 1, k \neq i\}$  and  $S^{k-} = \{s_{ki} = f(V_k, V_i) | V_i \in \mathcal{B}, Y_{ki} = 0\}$ , respectively. For the sake of presentation, let  $d_{ji}^k = s_{kj} - s_{ki}$ . According to Section 3.1, we aim to maximize the AP score, or equivalently minimize the following AP risk of the query video  $V_k$ :

$$AP_k^\downarrow(f) = 1 - AP_k(f) = \frac{1}{|S^{k+}|} \sum_{s_{ki} \in S^{k+}} \frac{\sum_{s_{kj} \in S^{k-}} \mathcal{H}(d_{ji}^k)}{1 + \sum_{s_{kj} \in S^{k+} \cup S^{k-}} \mathcal{H}(d_{ji}^k)}. \quad (6)$$

This AP risk is not differentiable due to the discontinuous function  $\mathcal{H}(\cdot)$ . To this end, previous methods such as Smooth-AP [4] employ the Sigmoid function (shown in Figure 4a) as a surrogate:

$$\mathcal{G}(x; \tau) = (1 + \exp(-x/\tau))^{-1} \approx \mathcal{H}(x), \quad (7)$$

which results in an approximation risk, i.e.,  $\widetilde{AP}_k^\downarrow(f)$ . When  $\tau \rightarrow 0$ , the  $\widetilde{AP}_k^\downarrow(f) \rightarrow AP_k^\downarrow(f)$ , thus the approximation error is small.

**Although Smooth-AP provides a straightforward solution to address the non-differentiable problem of AP, it might suffer from a gradient vanishing issue.**

Specifically, when the score of a negative instance  $s_{kj}$  significantly exceeds that of a positive instance  $s_{ki}$ , i.e.  $d_{ji}^k \gg 0$ ,  $d_{ji}^k$  falls into the gradient vanishing area of  $\mathcal{G}(x; \tau)$  as depicted in Figure 4b, i.e.  $\frac{d\mathcal{G}(x; \tau)}{dx} \Big|_{x=d_{ji}^k} \approx 0$ , leading to slow convergence and sub-optimal solutions. This phenomenon is more evident in video similarity learning since the partial matching property (see Section 3.3.1) makes  $d_{ji}^k$  more likely to fall into the gradient-vanishing area.

To avoid this issue, we aim to propose a novel AP loss. To begin with, we argue that it is unnecessary to replace all  $\mathcal{H}(\cdot)$ . Notice that the original AP risk in Appendix A.1 can be reformulated as:

$$AP_k^\downarrow(f) = \frac{1}{|S^{k+}|} \sum_{s_{ki} \in S^{k+}} h \left( \frac{\sum_{s_{kj} \in S^{k-}} \mathcal{H}(d_{ji}^k)}{1 + \sum_{s_{kj} \in S^{k+}} \mathcal{H}(d_{ji}^k)} \right), \quad (8)$$

where  $h(x) = \frac{x}{1+x}$  is a monotonically increasing function. Then, the non-differentiable terms  $\mathcal{H}(d_{ji}^k)$  can be divided into two types:

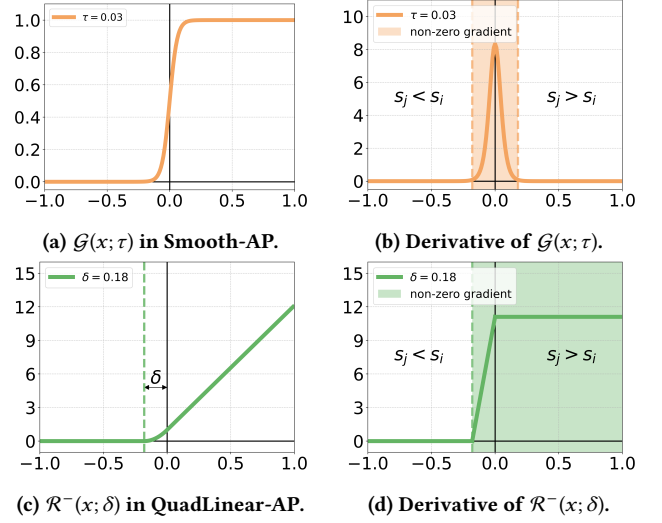


**Figure 4: The curves of Sigmoid function in Smooth-AP and surrogate loss function for positive-negative pairs in QuadLinear-AP and their derivative functions. The colored parts in (b) and (d) represent non-zero gradient areas.**

1) The positive-negative pair ( $s_{kj} \in S^{k-}$ ) in the numerator, which should be minimized to ensure the correct ranking; 2) The positive-positive pair ( $s_{kj} \in S^{k+}$ ) in the denominator, which plays a role of weights. From this perspective, we only need to ensure that the surrogate loss of the former has an appropriate gradient, while for the latter we can directly use the original rankings such that the importance of each term can be precisely measured.

Motivated by the above observation, for positive-positive pairs we still utilize the Heaviside function:

$$\mathcal{R}^+(x) = \mathcal{H}(x). \quad (9)$$

As for the positive-negative pairs, the derivative of the surrogate loss should be large for the wrongly ranked pairs, i.e.  $d_{ji}^k + \delta \geq 0$  for a given margin  $\delta > 0$ . Besides, the surrogate loss should be convex such that the derivative is (non-strictly) monotonically increasing. Therefore, we design the following surrogate loss for positive-negative pairs as displayed in Figure 4c:

$$\mathcal{R}^-(x; \delta) = \begin{cases} \mathcal{H}(-x) \cdot \frac{1}{\delta^2} x^2 + \frac{2}{\delta} x + 1, & \text{if } x \geq -\delta. \\ 0, & \text{if } x < -\delta. \end{cases} \quad (10)$$

As shown in Figure 4d,  $\mathcal{R}^-(x; \delta)$  still provides sufficient large gradients when  $d_{ji}^k \gg 0$ , and thereby forces the model to optimize  $f$  to correct mis-ranked pairs in an effective way. Obviously, the above surrogate loss satisfies our design principles. Furthermore, by introducing an extra parameter  $\rho$  to adjust the weight of positive-positive pairs, the score distribution between positive and negative instances can be balanced well. The analysis above induces the formulation of the following AP loss, namely QuadLinear-AP:

$$\widetilde{AP}_k^\downarrow(f) = \frac{1}{|S^{k+}|} \sum_{s_{ki} \in S^{k+}} h \left( \frac{\sum_{s_{kj} \in S^{k-}} \mathcal{R}^-(d_{ji}^k; \delta)}{1 + \rho \sum_{s_{kj} \in S^{k+}} \mathcal{R}^+(d_{ji}^k)} \right), \quad (11)$$

which enjoys the following properties (proved in Appendix A.2):

- **Differentiable AP optimization** QuadLinear-AP is differentiable for AP term, making it possible to backpropagate gradients in the learning process.
- **Suitable gradients for low AP area.** Persistent and suitable gradients in the loss function force model to correct wrongly ranked positive-negative pairs, avoiding gradient vanishing in the low AP area.
- **Favorable mathematical properties.** QuadLinear-AP is continuous, convex, and (non-strictly) monotonically increasing, ensuring a stable convergence during optimization.

As formulated in Eq. (12), the final AP loss is calculated by averaging QuadLinear-AP across all query videos. Clearly, this objective is aligned with the evaluation metric.

$$\mathcal{L}_{QLAP}^V = \frac{1}{N} \sum_{k=1}^N \widehat{AP}_k^\downarrow(f). \quad (12)$$

### 3.4 Frame Similarity Distillation

As discussed in Section 1, two relevant video instances may not be completely relevant at the frame level due to the noticeable variation in the temporal dimension, *i.e.*, only several frames are highly relevant with a query frame while the others are relatively low in actual. Therefore, solely optimizing  $f$  on video-level instances proves inadequate. Next, we dive into the frame-level learning.

Given a query frame, it is hard to locate the relevant frames from another video without fine-grained annotations. A possible route is leveraging self-distillation methods [8, 57], which refines image features by distilling ensemble information from a mean teacher to the target model in a self-supervised manner. Unfortunately, since our feature extractor  $g$  is trained with video data, it might ignore some image-level information. In this case, the pseudo labels generated by  $g$  cannot provide more informative supervision.

Consequently, we introduce another feature extractor  $g' : \mathcal{X} \mapsto \mathbb{R}^{T \times D'}$ , where  $D'$  is the embedding dimension. The feature extractor is pre-trained on image data with a self-supervised learning algorithm DINO [8], and the parameters are frozen. Given a video pair  $V, V'$ , we use  $g'$  to extract features for all frames and compute the following frame-level similarities, where  $V_x$  and  $V'_y$  are the  $x$ -th frame of  $V$  and  $y$ -th frame of  $V'$ , respectively.

$$S'(V, V')_{x,y} = \frac{g'(V_x)^\top g'(V'_y)}{\|g'(V_x)\|_2 \|g'(V'_y)\|_2}. \quad (13)$$

As shown in previous study [19], the similarities are highly correlated to the relevance. However, for different queries, the similarity distributions of its relevant/irrelevant frames are various, hence discretizing them into binary pseudo labels with fixed thresholds is impractical. Instead, we identify the frames with the highest/lowest similarities as positive/negative, leading to the pseudo labels:

$$\hat{Y}_{x,y} = \begin{cases} 1, & \text{if } S'(V, V')_{x,y} \geq S'(V, V')_{x,[r_t \times T]}, \\ 0, & \text{if } S'(V, V')_{x,y} \leq S'(V, V')_{x,[(1-r_b) \times T]}, \end{cases} \quad (14)$$

where  $r_t, r_b < 1$  are tunable hyperparameters,  $S'(V, V')_{x,[k]}$  refers to the  $k$ -th largest value in  $\{S'(V, V')_{x,y}\}_{y=1}^T$ .

Notice the varying similarity distributions across different video types, it's suboptimal to set a fixed threshold for positive or negative frames to exceed during the training phase. A feasible solution

is training the model to learn to rank positive frames above the negative ones. Resembling the method in video-level learning, we optimize the frame-level similarities by  $\mathcal{L}_{QLAP}^F$ , which can be implemented by substituting the video instances with frame instances.

Following previous methods on ranking optimization [13, 52], we combine a basic loss  $\mathcal{L}_{base}$  with the AP losses to promote collaborative optimization between ranking and representation learning. The basic loss comprises the InfoNCE loss [41] to support representation learning and an SSHN loss [33] for hard negative mining.

Ultimately, the total loss for hierarchical similarity learning is formulated in Eq. (15), where  $\lambda_f$  and  $\lambda_v$  are hyperparameters for the trade-off between components.

$$\mathcal{L} = \underbrace{\lambda_f \mathcal{L}_{QLAP}^F}_{\text{frame-level}} + \underbrace{\lambda_v \mathcal{L}_{QLAP}^V}_{\text{video-level}} + \mathcal{L}_{base} \quad (15)$$

## 4 EXPERIMENTS

In this section, we begin with a brief overview of the basic settings, including the datasets, evaluation metrics, and implementation details. Next, we compare our proposed learning framework with several previous methods on three benchmark datasets. Finally, we conduct an ablation study to evaluate the performance of different modules. For further details, please see the Appendix B.

### 4.1 Experimental Setup

**Datasets.** Our model is trained on the unlabeled subset of VCDB dataset[28] (we denote the core data and distractors as  $\mathcal{C}$  and  $\mathcal{D}$ , respectively) and evaluated on EVVE[48], SVD [27], and FIVR-5K/FIVR-200K [29]. For the FIVR dataset, we report the results of three specific subtasks: DSVR/DSVD, CSVr/CSVD, and ISVR/ISVD.

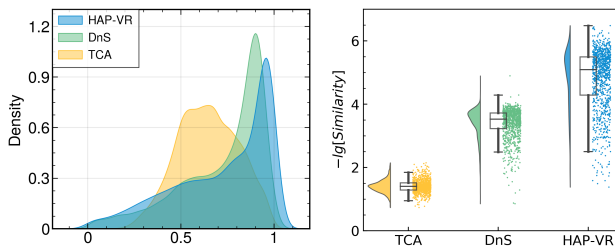
**Evaluation Metrics.** For retrieval tasks, we adopt Mean Average Precision (**mAP**) as the evaluation metric. Specifically, mAP calculates the average AP scores for each query independently and then averages these scores to reflect the model's overall ranking performance. For detection tasks, we employ Micro Average Precision ( **$\mu$ AP**), a metric widely used in previous studies [33, 35, 43, 44]. The  $\mu$ AP calculates the AP across all queries simultaneously, demonstrating the model's capability to consistently apply a uniform threshold across various queries to detect relevant instances.

**Implementation Details.** Given an input video, we generate two video clips by applying random augmentations that include temporal manipulations [30, 33], spatial transformations [12, 44], and other basic augmentations. For the feature extractor, we adopt ResNet50 [22] following [30, 33, 34], and for the pseudo label generator, we utilize DINO [8] pretrained ViT-small [15] with a patch size of 16. Our model is trained for 30,000 iterations with a batch size of 64. We use AdamW [39] with the Cosine Annealing scheduler for parameters optimization. The learning rate is set to  $4 \times 10^{-5}$  with a warm-up period [38], and weight decay is set to  $1 \times 10^{-2}$ .

**Competitors.** We evaluate HAP-VR against various leading video retrieval methods, categorized into two types. **1) Supervised methods** include DML [32], TMK [46], TCA [53], ViSiL [30], DnS [34] with both attention ( $S_a$ ) and binarization ( $S_b$ ) student network. **2) Unsupervised methods** include LAMV [2], VRL [24], ViSiL<sub>f</sub> [30] (untrained ViSiL baseline), and S<sup>2</sup>VS [33].

**Table 1: Comparison between video retrieval methods on EVVE, SVD, and FIVR-200K with mAP (%) of retrieval task and  $\mu$ AP (%) of detection task.  $\dagger$  indicates the results taken from the original paper. Missing values indicate the lack of implementation or original results. The first and second best results are highlighted in soft red and soft blue, respectively.**

Method	Label	Trainset	Retrieval (mAP)					Detection ( $\mu$ AP)				
			EVVE	SVD	FIVR-200K			EVVE	SVD	FIVR-200K		
					DSVR	CSVR	ISVR			DSVD	CSVD	ISVD
DML $\dagger$ [32]	✓	VCDB ( $C&D$ )	61.10	85.00	52.80	51.40	44.00	75.50	/	39.00	36.50	30.00
TMK $\dagger$ [46]	✓	internal	61.80	86.30	52.40	50.70	42.50	/	/	/	/	/
TCA [53]	✓	VCDB ( $C&D$ )	63.08	<b>89.82</b>	86.81	82.31	69.61	76.90	56.93	69.09	62.28	49.24
ViSiL $\dagger$ [30]	✓	VCDB ( $C&D$ )	65.80	88.10	89.90	85.40	72.30	79.10	/	75.80	69.00	53.00
DnS ( $S_a$ ) [34]	✓	DnS-100K	65.33	<b>90.20</b>	92.09	87.54	74.08	74.56	<b>72.24</b>	79.66	69.51	54.20
DnS ( $S_b$ ) [34]	✓	DnS-100K	64.41	89.12	90.89	86.28	72.87	75.80	66.53	78.05	68.52	53.48
LAMV $\dagger$ [2]	✗	YFCC100M	62.00	88.00	61.90	58.70	47.90	80.60	/	55.40	50.00	38.80
VRL $\dagger$ [24]	✗	internal	/	/	90.00	85.80	70.90	/	/	/	/	/
ViSiL $_f$ $\dagger$ [30]	✗	ImageNet	62.70	/	89.00	84.80	72.10	74.60	/	66.90	59.50	45.90
S <sup>2</sup> VS [33]	✗	VCDB ( $\mathcal{D}$ )	<b>67.17</b>	88.40	<b>92.53</b>	<b>87.73</b>	<b>74.51</b>	<b>80.72</b>	65.04	<b>86.12</b>	<b>77.41</b>	<b>63.26</b>
HAP-VR (Ours)	✗	VCDB ( $\mathcal{D}$ )	<b>69.15</b>	89.00	<b>92.83</b>	<b>88.21</b>	<b>74.72</b>	<b>82.88</b>	<b>67.87</b>	<b>88.41</b>	<b>79.85</b>	<b>64.79</b>



(a) Relevant pair distribution. (b) Irrelevant pair distribution.

**Figure 5: Video similarity distribution of relevant and irrelevant instance pairs for HAP-VR, DnS, and TCA on the DSVD set of FIVR-200K. All similarities are rescaled to [0, 1].**

## 4.2 Evaluation Results

The overall performance on video retrieval and detection tasks above is reported in Table 1, leading to several key conclusions: **1)** HAP-VR stands out among other unsupervised or self-supervised methods in both mAP and  $\mu$ AP metrics, with an average improvement of **0.71%** and **2.25%**, respectively. These outcomes underscore the effectiveness of aligning the training objectives with the evaluation metrics, directly enhancing the average precision. **2)** Detection tasks enjoy larger performance gains than retrieval tasks. This is primarily due to the more pronounced imbalance between instances in detection tasks. By emphasizing the overall rankings of the positive instances, HAP-VR achieves a more optimal similarity distribution across all queries, resulting in a notable increase in  $\mu$ AP. **3)** Compared with supervised methods, HAP-VR achieves a better overall performance. To investigate the underlying reason, we visualize the similarity distributions in Figure 5. Compared with the supervised methods, HAP-VR establishes a clearer margin between scores of relevant and irrelevant pairs. Since annotations are based

on the video categories, the supervised model tends to distinguish the pre-defined categories but not video instances. Accordingly, when encountering videos beyond these pre-defined categories, the model is prone to overfitting, which hinders discriminating between negative instances, thereby reducing the model’s transferability.

## 4.3 Ablation Study

**Ablation results on proposed QuadLinear-AP loss.** To validate the effectiveness of the proposed QuadLinear-AP loss, we make a comparison with other commonly used losses, which can be categorized into three types: **1) Point-wise losses**, include Mean Absolute Error (MAE) and Mean Squared Error (MSE). These losses measure the discrepancy between predicted scores and actual labels for each item independently. **2) Pair-wise losses**, include Contrastive loss [18], Triplet loss [50] and Circle loss [55]. These losses focus on distinguishing between the positive and negative instances in pairs. **3) List-wise losses**, include FastAP [6], DIR [47], BlackBox [45], and Smooth-AP [4]. These approaches optimize the model directly based on ranking metrics such as AP.

For a straightforward comparison, we only combine these losses with  $\mathcal{L}_{base}$  and train the models using 10% of the VCDB ( $\mathcal{D}$ ) for 10,000 iterations. Except for the specific hyperparameters associated with each loss, all other settings remain constant to ensure a fair comparison. The comparison results are presented in Table 2. From these results, we can draw the following conclusions: **1)** In general, list-wise losses outperform point-wise and pair-wise losses, supporting our motivation to develop an AP-oriented method for video retrieval tasks. **2)** QuadLinear-AP achieves an average improvement of about **1.84%** on mAP and **2.87%** on  $\mu$ AP over other list-wise losses, reflecting the effectiveness of the proposed AP loss. The visualization of frame-level similarity shown in Figure 6 illustrates that QuadLinear-AP presents a clearer distinction between relevant and irrelevant instances compared to other competitors.

**Table 2: Comparison between QuadLinear-AP and other loss functions on the FIVR-5K with mAP (%) of retrieval task and  $\mu$ AP (%) of detection task. The first and second best results are highlighted in soft red and soft blue, respectively.**

Losses	Retrieval (mAP)			Detection ( $\mu$ AP)		
	DSVR	CSVR	ISVR	DSVD	CSVD	ISVD
MAE	89.07	88.03	80.86	78.08	75.69	65.26
MSE	89.22	88.26	80.80	78.66	76.07	65.44
Contrastive [18]	88.67	88.09	80.97	75.12	74.23	67.41
Triplet [50]	88.11	87.77	<b>81.21</b>	72.94	73.18	69.23
Circle [55]	87.53	86.11	78.77	73.26	71.15	59.33
FastAP [6]	89.30	88.42	81.16	78.83	77.51	<b>69.95</b>
DIR [47]	89.65	<b>88.57</b>	80.64	78.50	76.22	65.42
BlackBox [45]	<b>89.70</b>	88.55	80.53	<b>80.07</b>	77.37	66.00
Smooth-AP [4]	89.36	88.33	80.73	79.85	<b>77.75</b>	68.42
QuadLinear-AP (Ours)	<b>90.80</b>	<b>89.68</b>	<b>81.31</b>	<b>82.92</b>	<b>80.03</b>	<b>71.45</b>

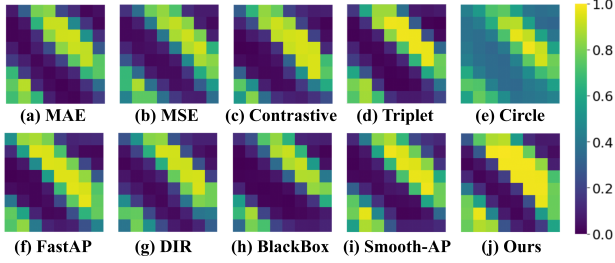


**Figure 6: Heatmaps of similarity matrices generated by various losses. In contrast, our QuadLinear-AP distinguishes between relevant and irrelevant instances more clearly.**

**Ablation results on proposed modules.** Comparing Line 1 with Line 2 in Table 3, the application of the TopK-Chamfer Similarity measure yields average boosts of **0.59%** on mAP and **1.13%** on  $\mu$ AP based on the baseline model, demonstrating its efficacy. Comparing Line 2 with Line 3 shows that incorporating video-level AP optimization enhances retrieval and detection performance with increases of **0.69%** and **2.13%** respectively. Such improvements reveal the necessity of aligning training objectives with evaluation metrics. Moreover, implementing a frame-level learning process further improves the overall outcomes, emphasizing the value of learning the internal similarity within the video precisely.

**Ablation results on similarity measure.** To validate the effectiveness of the proposed TopK-Chamfer Similarity measure, we evaluate the model varying the top-k rate  $k_t$ . Note that when  $k_t = 0.0$ , the measure can be seen as the original Chamfer Similarity; when  $k_t = 1.0$ , the measure is equal to average pooling. As indicated in Table 4, the optimal performance is achieved neither at  $k_t = 0.0$  nor at  $k_t = 1.0$ . This outcome supports the utility of selecting top-K values. From another perspective, the best performance is obtained when  $k_t$  is small, demonstrating the capability of the TopK-Chamfer Similarity in diminishing redundancy and reducing the influence of noise, thereby ensuring robustness in similarity calculation.

**Table 3: Results in the ablation study of modules including TopK-Chamfer Similarity measure, video-level AP loss, and frame-level AP loss. Improvements in performance compared to the baseline are denoted with red subscripts.**

$\mathcal{L}_{base}$	TopK. Sim.	$\mathcal{L}_{QLAP}^V$	$\mathcal{L}_{QLAP}^F$	EVVE	FIVR-5K		
					DSVR/DSVD	CSVR/CSVD	ISVR/ISVD
<b>Retrieval (mAP)</b>							
✓				67.64	88.18	87.16	80.14
✓	✓			69.41 <sub>+1.77</sub>	88.36 <sub>+0.18</sub>	87.42 <sub>+0.26</sub>	80.30 <sub>+0.16</sub>
✓	✓	✓		69.55 <sub>+1.91</sub>	89.39 <sub>+1.21</sub>	88.54 <sub>+1.38</sub>	80.79 <sub>+0.65</sub>
✓	✓	✓	✓	69.58 <sub>+1.94</sub>	89.75 <sub>+1.57</sub>	88.59 <sub>+1.43</sub>	80.72 <sub>+0.58</sub>
<b>Detection (<math>\mu</math>AP)</b>							
✓				79.13	75.49	73.84	63.50
✓	✓			80.67 <sub>+1.54</sub>	76.23 <sub>+0.74</sub>	74.77 <sub>+0.93</sub>	64.81 <sub>+1.31</sub>
✓	✓	✓		81.09 <sub>+1.96</sub>	78.64 <sub>+3.15</sub>	77.04 <sub>+3.20</sub>	68.23 <sub>+4.73</sub>
✓	✓	✓	✓	82.96 <sub>+3.83</sub>	81.56 <sub>+6.07</sub>	78.32 <sub>+4.48</sub>	66.87 <sub>+3.37</sub>

**Table 4: Results in the ablation study of similarity measure. In particular, \* represents using Chamfer Similarity and  $\dagger$  represents using average pooling. The first and second best results are highlighted in soft red and soft blue, respectively.**

$k_t$	Retrieval (mAP)				Detection ( $\mu$ AP)			
	EVVE	FIVR-5K			EVVE	FIVR-5K		
		DSVR	CSVR	ISVR		DSVD	CSVD	ISVD
0.00*	67.57	<b>89.52</b>	88.38	80.55	78.85	<b>78.78</b>	76.93	65.99
0.03	68.98	<b>89.65</b>	<b>88.69</b>	<b>80.91</b>	80.70	<b>79.01</b>	<b>77.01</b>	<b>68.21</b>
0.06	<b>69.55</b>	89.39	<b>88.54</b>	<b>80.79</b>	<b>81.09</b>	78.64	<b>77.04</b>	<b>68.23</b>
0.10	<b>69.03</b>	87.87	87.12	79.69	80.75	73.19	71.75	61.96
0.20	68.69	85.26	85.01	78.01	<b>81.54</b>	69.12	68.35	59.57
0.30	68.27	81.54	81.98	75.93	80.04	64.30	65.41	58.41
1.00 $\dagger$	55.49	61.29	64.25	62.84	77.32	37.57	44.27	42.92

## 5 CONCLUSION

In this paper, we design a self-supervised framework for video retrieval, which features a video-oriented similarity measure to gather fine-grained features and a novel AP-based loss with reasonable gradients to correct mis-ranked instance pairs efficiently, filling the gap between the training objective and evaluation metric. Within the framework, we propose a hierarchical learning strategy to optimize AP on both video and frame levels, resulting in precise estimations of the AP loss and thus improving the accuracy of similarity learning. Experimental results demonstrate that our framework often surpasses previous works in several benchmark datasets, making it a feasible solution for video retrieval tasks.

## ACKNOWLEDGMENTS

This work was supported in part by the National Key R&D Program of China under Grant 2018AAA0102000, in part by National Natural Science Foundation of China: 62236008, U21B2038, U23B2051, 61931008, 62122075 and 61976202, in part by Youth Innovation Promotion Association CAS, in part by the Strategic Priority Research Program of the Chinese Academy of Sciences, Grant No. XDB0680000, in part by the Innovation Funding of ICT, CAS under Grant No.E000000.



## REFERENCES

- [1] Aasif Ansari and Muzammil H Mohammed. 2015. Content based video retrieval systems-methods, techniques, trends and challenges. *International Journal of Computer Applications* 112, 7 (2015).
- [2] Lorenzo Baraldi, Matthijs Douze, Rita Cucchiara, and Hervé Jégou. 2018. LAMV: Learning to align and match videos with kernelized temporal layers. In *IEEE/CVF Conference on Computer Vision and Pattern Recognition*. 7804–7813.
- [3] Harry G Barrow, Jay M Tenenbaum, Robert C Bolles, and Helen C Wolf. 1977. Parametric correspondence and chamfer matching: Two new techniques for image matching. In *Proceedings: Image Understanding Workshop*. Science Applications, Inc, 21–27.
- [4] Andrew Brown, Weidi Xie, Vicky Kalogeiton, and Andrew Zisserman. 2020. Smooth-ap: Smoothing the path towards large-scale image retrieval. In *European Conference on Computer Vision*. Springer, 677–694.
- [5] Yang Cai, Linjun Yang, Wei Ping, Fei Wang, Tao Mei, Xian-Sheng Hua, and Shipeng Li. 2011. Million-scale near-duplicate video retrieval system. In *ACM International Conference on Multimedia*. 837–838.
- [6] Fatih Cakir, Kun He, Xide Xia, Brian Kulis, and Stan Sclaroff. 2019. Deep metric learning to rank. In *IEEE/CVF Conference on Computer Vision and Pattern Recognition*. 1861–1870.
- [7] Zhe Cao, Tao Qin, Tie-Yan Liu, Ming-Feng Tsai, and Hang Li. 2007. Learning to rank: from pairwise approach to listwise approach. In *International Conference on Machine Learning*. 129–136.
- [8] Mathilde Caron, Hugo Touvron, Ishan Misra, Hervé Jégou, Julien Mairal, Piotr Bojanowski, and Armand Joulin. 2021. Emerging properties in self-supervised vision transformers. In *International Conference on Computer Vision*. 9650–9660.
- [9] Ting Chen, Simon Kornblith, Mohammad Norouzi, and Geoffrey Hinton. 2020. A simple framework for contrastive learning of visual representations. In *International Conference on Machine Learning*. PMLR, 1597–1607.
- [10] Sumit Chopra, Raia Hadsell, and Yann LeCun. 2005. Learning a similarity metric discriminatively, with application to face verification. In *IEEE/CVF Conference on Computer Vision and Pattern Recognition*, Vol. 1. IEEE, 539–546.
- [11] Chien-Li Chou, Hua-Tsung Chen, and Suh-Yin Lee. 2015. Pattern-based near-duplicate video retrieval and localization on web-scale videos. *IEEE Transactions on Multimedia* 17, 3 (2015), 382–395.
- [12] Ekin D Cubuk, Barret Zoph, Jonathon Shlens, and Quoc V Le. 2020. Randaugment: Practical automated data augmentation with a reduced search space. In *IEEE/CVF Conference on Computer Vision and Pattern Recognition Workshop*. 702–703.
- [13] Siran Dai, Qianqian Xu, Zhiyong Yang, Xiaochun Cao, and Qingming Huang. 2024. DRAUC: An Instance-wise Distributionally Robust AUC Optimization Framework. *Advances in Neural Information Processing Systems* 36 (2024).
- [14] Jia Deng, Wei Dong, Richard Socher, Li-Jia Li, Kai Li, and Li-Fei-Fei. 2009. Imagenet: A large-scale hierarchical image database. In *IEEE/CVF Conference on Computer Vision and Pattern Recognition*. IEEE, 248–255.
- [15] Alexey Dosovitskiy, Lucas Beyer, Alexander Kolesnikov, Dirk Weissenborn, Xi-aohua Zhai, Thomas Unterthiner, Mostafa Dehghani, Matthias Minderer, Georg Heigold, Sylvain Gelly, et al. 2020. An image is worth 16x16 words: Transformers for image recognition at scale. *arXiv preprint arXiv:2010.11929* (2020).
- [16] Matthijs Douze, Hervé Jégou, and Cordelia Schmid. 2010. An image-based approach to video copy detection with spatio-temporal post-filtering. *IEEE Transactions on Multimedia* 12, 4 (2010), 257–266.
- [17] Yang Feng, Lin Ma, Wei Liu, Tong Zhang, and Jiebo Luo. 2018. Video re-localization. In *European Conference on Computer Vision*. 51–66.
- [18] Raia Hadsell, Sumit Chopra, and Yann LeCun. 2006. Dimensionality reduction by learning an invariant mapping. In *IEEE/CVF Conference on Computer Vision and Pattern Recognition*, Vol. 2. IEEE, 1735–1742.
- [19] Mark Hamilton, Zhoutong Zhang, Bharath Hariharan, Noah Snavely, and William T Freeman. 2022. Unsupervised Semantic Segmentation by Distilling Feature Correspondences. In *International Conference on Learning Representations*.
- [20] Tamir Hazan, Joseph Keshet, and David McAllester. 2010. Direct loss minimization for structured prediction. *Advances in Neural Information Processing Systems* 23 (2010).
- [21] Kaiming He, Haoqi Fan, Yuxin Wu, Saining Xie, and Ross Girshick. 2020. Momentum contrast for unsupervised visual representation learning. In *IEEE/CVF Conference on Computer Vision and Pattern Recognition*. 9729–9738.
- [22] Kaiming He, Xiangyu Zhang, Shaoqing Ren, and Jian Sun. 2016. Deep residual learning for image recognition. In *IEEE/CVF Conference on Computer Vision and Pattern Recognition*. 770–778.
- [23] Sifeng He, Yue He, Minlong Lu, Chen Jiang, Xudong Yang, Feng Qian, Xiaobo Zhang, Lei Yang, and Jiandong Zhang. 2023. TransVCL: attention-enhanced video copy localization network with flexible supervision. In *Association for the Advancement of Artificial Intelligence*, Vol. 37. 799–807.
- [24] Xiangteng He, Yulin Pan, Mingqian Tang, Yiliang Lv, and Yuxin Peng. 2022. Learn from unlabeled videos for near-duplicate video retrieval. In *International ACM SIGIR Conference on Research and Development in Information Retrieval*. 1002–1011.
- [25] Olivier Henaff. 2020. Data-efficient image recognition with contrastive predictive coding. In *International Conference on Machine Learning*. PMLR, 4182–4192.
- [26] Weiming Hu, Nianhua Xie, Li Li, Xianglin Zeng, and Stephen Maybank. 2011. A survey on visual content-based video indexing and retrieval. *IEEE Transactions on Systems, Man, and Cybernetics, Part C (Applications and Reviews)* 41, 6 (2011), 797–819.
- [27] Qing-Yuan Jiang, Yi He, Gen Li, Jian Lin, Lei Li, and Wu-Jun Li. 2019. SVD: A large-scale short video dataset for near-duplicate video retrieval. In *International Conference on Computer Vision*. 5281–5289.
- [28] Yu-Gang Jiang, Yudong Jiang, and Jiajun Wang. 2014. VCDB: a large-scale database for partial copy detection in videos. In *European Conference on Computer Vision*. Springer, 357–371.
- [29] Giorgos Kordopatis-Zilos, Symeon Papadopoulos, Ioannis Patras, and Ioannis Kompatsiaris. 2019. FIVR: Fine-grained incident video retrieval. *IEEE Transactions on Multimedia* 21, 10 (2019), 2638–2652.
- [30] Giorgos Kordopatis-Zilos, Symeon Papadopoulos, Ioannis Patras, and Ioannis Kompatsiaris. 2019. Visil: Fine-grained spatio-temporal video similarity learning. In *International Conference on Computer Vision*. 6351–6360.
- [31] Giorgos Kordopatis-Zilos, Symeon Papadopoulos, Ioannis Patras, and Yiannis Kompatsiaris. 2017. Near-duplicate video retrieval by aggregating intermediate cnn layers. In *MultiMedia Modeling: 23rd International Conference, MMM 2017, Reykjavik, Iceland, January 4-6, 2017, Proceedings, Part I 23*. Springer, 251–263.
- [32] Giorgos Kordopatis-Zilos, Symeon Papadopoulos, Ioannis Patras, and Yiannis Kompatsiaris. 2017. Near-duplicate video retrieval with deep metric learning. In *Proceedings of the IEEE International Conference on Computer Vision workshops*. 347–356.
- [33] Giorgos Kordopatis-Zilos, Giorgos Tolias, Christos Tzelepis, Ioannis Kompatsiaris, Ioannis Patras, and Symeon Papadopoulos. 2023. Self-Supervised Video Similarity Learning. In *IEEE/CVF Conference on Computer Vision and Pattern Recognition*. 4755–4765.
- [34] Giorgos Kordopatis-Zilos, Christos Tzelepis, Symeon Papadopoulos, Ioannis Kompatsiaris, and Ioannis Patras. 2022. DnS: Distill-and-select for efficient and accurate video indexing and retrieval. *International Journal of Computer Vision* 130, 10 (2022), 2385–2407.
- [35] Julien Law-To, Li Chen, Alexis Joly, Ivan Laptev, Olivier Buisson, Valerie Gouet-Brunet, Nozha Boujemaa, and Fred Stentiford. 2007. Video copy detection: a comparative study. In *Proceedings of the 6th ACM international conference on Image and video retrieval*. 371–378.
- [36] Joonseok Lee, Sami Abu-El-Hajja, Balakrishnan Varadarajan, and Apostol Natsev. 2018. Collaborative deep metric learning for video understanding. In *Proceedings of the 24th ACM SIGKDD International conference on knowledge discovery and data mining*. 481–490.
- [37] Kaiyang Liao, Hao Lei, Yuanlin Zheng, Guangfeng Lin, Congjun Cao, Mingzhu Zhang, and Jie Ding. 2018. IR feature embedded bof indexing method for near-duplicate video retrieval. *IEEE Transactions on Circuits and Systems for Video Technology* 29, 12 (2018), 3743–3753.
- [38] Ilya Loshchilov and Frank Hutter. 2016. SGDR: Stochastic Gradient Descent with Warm Restarts. In *International Conference on Learning Representations*.
- [39] Ilya Loshchilov and Frank Hutter. 2018. Decoupled Weight Decay Regularization. In *International Conference on Learning Representations*.
- [40] Pritish Mohapatra, CV Jawahar, and M Pawan Kumar. 2014. Efficient optimization for average precision svm. *Advances in Neural Information Processing Systems* 27 (2014).
- [41] Aaron van den Oord, Yazhe Li, and Oriol Vinyals. 2018. Representation learning with contrastive predictive coding. *arXiv preprint arXiv:1807.03748* (2018).
- [42] Adam Paszke, Sam Gross, Francisco Massa, Adam Lerer, James Bradbury, Gregory Chanan, Trevor Killeen, Zeming Lin, Natalia Gimelshein, Luca Antiga, et al. 2019. Pytorch: An imperative style, high-performance deep learning library. *Advances in Neural Information Processing Systems* 32 (2019).
- [43] Florent Perronnin, Yan Liu, and Jean-Michel Renders. 2009. A family of contextual measures of similarity between distributions with application to image retrieval. In *IEEE/CVF Conference on Computer Vision and Pattern Recognition*. IEEE, 2358–2365.
- [44] Ed Pizzi, Sreya Dutta Roy, Sugosh Nagavara Ravindra, Priya Goyal, and Matthijs Douze. 2022. A self-supervised descriptor for image copy detection. In *IEEE/CVF Conference on Computer Vision and Pattern Recognition*. 14532–14542.
- [45] Marin Vlastelica Pogančić, Anselm Paulus, Vit Musil, Georg Martius, and Michal Rolínek. 2019. Differentiation of blackbox combinatorial solvers. In *International Conference on Learning Representations*.
- [46] Sébastien Poullot, Shunsuke Tsukatani, Anh Phuong Nguyen, Hervé Jégou, and Shin'Ichi Satoh. 2015. Temporal matching kernel with explicit feature maps. In *ACM International Conference on Multimedia*. 381–390.
- [47] Jerome Revaud, Jon Almazán, Rafael S Rezende, and Cesar Roberto de Souza. 2019. Learning with average precision: Training image retrieval with a listwise loss. In *International Conference on Computer Vision*. 5107–5116.
- [48] Jérôme Revaud, Matthijs Douze, Cordelia Schmid, and Hervé Jégou. 2013. Event retrieval in large video collections with circulant temporal encoding. In *IEEE/CVF Conference on Computer Vision and Pattern Recognition*. 2459–2466.

- [49] Michal Rolínek, Vít Musil, Anselm Paulus, Marin Vlastelica, Claudio Michaelis, and Georg Martius. 2020. Optimizing rank-based metrics with blackbox differentiation. In *IEEE/CVF Conference on Computer Vision and Pattern Recognition*. 7620–7630.
- [50] Florian Schroff, Dmitry Kalenichenko, and James Philbin. 2015. Facenet: A unified embedding for face recognition and clustering. In *IEEE/CVF Conference on Computer Vision and Pattern Recognition*. 815–823.
- [51] Lifeng Shang, Linjun Yang, Fei Wang, Kwok-Ping Chan, and Xian-Sheng Hua. 2010. Real-time large scale near-duplicate web video retrieval. In *ACM International Conference on Multimedia*. 531–540.
- [52] Huiyang Shao, Qianqian Xu, Zhiyong Yang, Peisong Wen, Gao Peifeng, and Qingming Huang. 2024. Weighted roc curve in cost space: Extending auc to cost-sensitive learning. *Advances in Neural Information Processing Systems* 36 (2024).
- [53] Jie Shao, Xin Wen, Bingchen Zhao, and Xiangyang Xue. 2021. Temporal context aggregation for video retrieval with contrastive learning. In *Proceedings of the IEEE/CVF winter conference on applications of computer vision*. 3268–3278.
- [54] Yang Song, Alexander Schwing, Raquel Urtasun, et al. 2016. Training deep neural networks via direct loss minimization. In *International Conference on Machine Learning*. PMLR, 2169–2177.
- [55] Yifan Sun, Changmao Cheng, Yuhang Zhang, Chi Zhang, Liang Zheng, Zhongdao Wang, and Yichen Wei. 2020. Circle loss: A unified perspective of pair similarity optimization. In *IEEE/CVF Conference on Computer Vision and Pattern Recognition*. 6398–6407.
- [56] Hung-Khoon Tan, Chong-Wah Ngo, Richard Hong, and Tat-Seng Chua. 2009. Scalable detection of partial near-duplicate videos by visual-temporal consistency. In *ACM International Conference on Multimedia*. 145–154.
- [57] Antti Tarvainen and Harri Valpola. 2017. Mean teachers are better role models: Weight-averaged consistency targets improve semi-supervised deep learning results. *Advances in Neural Information Processing Systems* 30 (2017).
- [58] Evgeniya Ustinova and Victor Lempitsky. 2016. Learning deep embeddings with histogram loss. *Advances in Neural Information Processing Systems* 29 (2016).
- [59] Ling Wang, Yu Bao, Haojie Li, Xin Fan, and Zhongxuan Luo. 2017. Compact CNN based video representation for efficient video copy detection. In *MultiMedia Modeling: 23rd International Conference, MMM 2017, Reykjavik, Iceland, January 4-6, 2017, Proceedings, Part I 23*. Springer, 576–587.
- [60] Zitai Wang, Qianqian Xu, Zhiyong Yang, Yuan He, Xiaochun Cao, and Qingming Huang. 2022. Openauc: Towards auc-oriented open-set recognition. *Advances in Neural Information Processing Systems* 35 (2022), 25033–25045.
- [61] Zitai Wang, Qianqian Xu, Zhiyong Yang, Yuan He, Xiaochun Cao, and Qingming Huang. 2022. Optimizing partial area under the top-k curve: Theory and practice. *IEEE Transactions on Pattern Analysis and Machine Intelligence* 45, 4 (2022), 5053–5069.
- [62] Kilian Q Weinberger and Lawrence K Saul. 2009. Distance metric learning for large margin nearest neighbor classification. *Journal of machine learning research* 10, 2 (2009).
- [63] Peisong Wen, Qianqian Xu, Zhiyong Yang, Yuan He, and Qingming Huang. 2022. Exploring the algorithm-dependent generalization of auprc optimization with list stability. *Advances in Neural Information Processing Systems* 35 (2022), 28335–28349.
- [64] Peisong Wen, Qianqian Xu, Zhiyong Yang, Yuan He, and Qingming Huang. 2024. Algorithm-Dependent Generalization of AUPRC Optimization: Theory and Algorithm. *IEEE Transactions on Pattern Analysis and Machine Intelligence* (2024).
- [65] Qianqian Xu, Zhiyong Yang, Yangbangyan Jiang, Xiaochun Cao, Yuan Yao, and Qingming Huang. 2020. Not all samples are trustworthy: Towards deep robust svp prediction. *IEEE Transactions on Pattern Analysis and Machine Intelligence* 44, 6 (2020), 3154–3169.
- [66] Zhiyong Yang, Qianqian Xu, Shilong Bao, Xiaochun Cao, and Qingming Huang. 2021. Learning with multiclass AUC: Theory and algorithms. *IEEE Transactions on Pattern Analysis and Machine Intelligence* 44, 11 (2021), 7747–7763.
- [67] Zhiyong Yang, Qianqian Xu, Shilong Bao, Yuan He, Xiaochun Cao, and Qingming Huang. 2022. Optimizing two-way partial auc with an end-to-end framework. *IEEE Transactions on Pattern Analysis and Machine Intelligence* 45, 8 (2022), 10228–10246.
- [68] Yisong Yue, Thomas Finley, Filip Radlinski, and Thorsten Joachims. 2007. A support vector method for optimizing average precision. In *International ACM SIGIR Conference on Research and Development in Information Retrieval*. 271–278.
- [69] Weihong Zhang and Ying Zhou. 2020. *The feature-driven method for structural optimization*. Elsevier.

## APPENDIX

<b>A Additional Illustration of Method</b>	<b>11</b>
A.1 Derivation of AP Risk . . . . .	11
A.2 Proofs of QuadLinear-AP's properties . . . . .	11
A.2.1 Differentiability . . . . .	11
A.2.2 Smoothness . . . . .	11
A.2.3 Convexity . . . . .	11
A.2.4 Non-strictly Monotonically Increasing . . . . .	12
A.2.5 Upper Bound of Heaviside Function . . . . .	12
A.3 Description of the Basic Loss . . . . .	12
A.4 Hierarchical Average Precision Optimization Algorithm . . . . .	12
<b>B Detailed Description of Experiments</b>	<b>12</b>
B.1 Datasets . . . . .	12
B.2 Evaluation Metrics . . . . .	13
B.3 Implementation Details . . . . .	13
B.4 Additional Ablation Study . . . . .	14
<b>C Visualization</b>	<b>15</b>

## A ADDITIONAL ILLUSTRATION OF METHOD

### A.1 Derivation of AP Risk

In a batch of videos  $\mathcal{B} = \{V_i \in \mathcal{X}\}_{i=1}^N$ , recall that for a query video  $V_k$ , the similarity scores of the relevant/irrelevant videos are denoted as  $S^{k+}/S^{k-}$ . For simplicity, let  $d_{ji}^k = s_{kj} - s_{ki}$ . As mentioned in Section 3.1, our goal is to maximize the AP score. This is achieved by minimizing the AP risk, which is derived as follows:

$$\begin{aligned}
 AP_k^\downarrow(f) &= 1 - AP_k(f) \\
 &= 1 - \frac{1}{|S^{k+}|} \sum_{s_{ki} \in S^{k+}} \frac{\mathcal{R}(s_{ki}, S^{k+})}{\mathcal{R}(s_{ki}, S^{k+} \cup S^{k-})} \\
 &= 1 - \frac{1}{|S^{k+}|} \sum_{s_{ki} \in S^{k+}} \frac{1 + \sum_{s_{kj} \in S^{k+}} \mathcal{H}(d_{ji}^k)}{1 + \sum_{s_{kj} \in S^{k+} \cup S^{k-}} \mathcal{H}(d_{ji}^k)} \\
 &= \frac{1}{|S^{k+}|} \sum_{s_{ki} \in S^{k+}} \frac{\sum_{s_{kj} \in S^{k-}} \mathcal{H}(d_{ji}^k)}{1 + \sum_{s_{kj} \in S^{k+} \cup S^{k-}} \mathcal{H}(d_{ji}^k)} \\
 &= \frac{1}{|S^{k+}|} \sum_{s_{ki} \in S^{k+}} \frac{\sum_{s_{kj} \in S^{k-}} \mathcal{H}(d_{ji}^k)}{1 + \sum_{s_{kj} \in S^{k+}} \mathcal{H}(d_{ji}^k) + \sum_{s_{kj} \in S^{k-}} \mathcal{H}(d_{ji}^k)} \\
 &= \frac{1}{|S^{k+}|} \sum_{s_{ki} \in S^{k+}} \frac{[\sum_{s_{kj} \in S^{k-}} \mathcal{H}(d_{ji}^k)] / [1 + \sum_{s_{kj} \in S^{k+}} \mathcal{H}(d_{ji}^k)]}{1 + [\sum_{s_{kj} \in S^{k-}} \mathcal{H}(d_{ji}^k)] / [1 + \sum_{s_{kj} \in S^{k+}} \mathcal{H}(d_{ji}^k)]} \\
 &= \frac{1}{|S^{k+}|} \sum_{s_{ki} \in S^{k+}} h\left(\frac{\sum_{s_{kj} \in S^{k-}} \mathcal{H}(d_{ji}^k)}{1 + \sum_{s_{kj} \in S^{k+}} \mathcal{H}(d_{ji}^k)}\right),
 \end{aligned}$$

where  $\mathcal{R}(s, S) = 1 + \sum_{s' \in S} \mathcal{H}(s' - s)$  is the descending ranking of  $s$  in  $S$ ,  $\mathcal{H}(\cdot)$  is the Heaviside function,  $h(x) = \frac{x}{1+x}$  is a monotonically increasing function.

We substitute the Heaviside function in the numerator with  $\mathcal{R}^-(d_{ji}^k; \delta)$  in eq.(10) and introduce an additional parameter  $\rho$ , which forms the following surrogate AP risk:

$$\widehat{AP}_k^\downarrow(f) = \frac{1}{|S^{k+}|} \sum_{s_{ki} \in S^{k+}} h\left(\frac{\sum_{s_{kj} \in S^{k-}} \mathcal{R}^-(d_{ji}^k; \delta)}{1 + \rho \sum_{s_{kj} \in S^{k+}} \mathcal{H}(d_{ji}^k)}\right).$$

### A.2 Proofs of QuadLinear-AP's properties

In this subsection, we provide proofs for several properties of QuadLinear-AP as outlined in Section 3.3 of the main paper. Specifically, we focus on the proofs of  $\mathcal{R}^-(x; \delta)$  since it determines these properties of QuadLinear-AP.

**A.2.1 Differentiability.** Note that it is unnecessary to replace  $\mathcal{H}(\cdot)$  for the positive-positive pair since it only plays a role of weight for precisely measuring each term in eq. (8). Therefore, we only need to ensure the  $\mathcal{R}^-(x; \delta)$  is differentiable, which is proved as follows.

First, the  $\mathcal{R}^-(x; \delta)$  can be reformatted as:

$$\mathcal{R}^-(x; \delta) = \begin{cases} \frac{2}{\delta}x + 1, & \text{if } x \geq 0. \\ \frac{1}{\delta^2}x^2 + \frac{2}{\delta}x + 1, & \text{if } -\delta \leq x < 0. \\ 0, & \text{if } x < -\delta. \end{cases}$$

Clearly,  $\mathcal{R}^-(x; \delta)$  is differentiable on its three segments. Now, we only need to verify that it is differentiable at the points where  $x = -\delta$  and  $x = 0$ .

When  $x = -\delta$ , we have:

$$\begin{aligned}
 \frac{d\mathcal{R}^-(x^-; \delta)}{dx^-} &= \lim_{x^- \rightarrow -\delta} \frac{\mathcal{R}^-(x^-; \delta) - \mathcal{R}^-(-\delta; \delta)}{x^- - (-\delta)} = 0, \\
 \frac{d\mathcal{R}^-(x^+; \delta)}{dx^+} &= \lim_{x^+ \rightarrow -\delta} \frac{\mathcal{R}^-(x^+; \delta) - \mathcal{R}^-(-\delta; \delta)}{x^+ - (-\delta)} = 0, \\
 \frac{d\mathcal{R}^-(x^-; \delta)}{dx^-} &= \frac{d\mathcal{R}^-(x^+; \delta)}{dx^+} = \frac{d\mathcal{R}^-(x; \delta)}{dx} \Big|_{x=-\delta} = 0.
 \end{aligned}$$

When  $x = 0$ , we have:

$$\begin{aligned}
 \frac{d\mathcal{R}^-(x^-; \delta)}{dx^-} &= \lim_{x^- \rightarrow 0} \frac{\mathcal{R}^-(x^-; \delta) - \mathcal{R}^-(0; \delta)}{x^- - 0} = \frac{2}{\delta}, \\
 \frac{d\mathcal{R}^-(x^+; \delta)}{dx^+} &= \lim_{x^+ \rightarrow 0} \frac{\mathcal{R}^-(x^+; \delta) - \mathcal{R}^-(0; \delta)}{x^+ - 0} = \frac{2}{\delta}, \\
 \frac{d\mathcal{R}^-(x^-; \delta)}{dx^-} &= \frac{d\mathcal{R}^-(x^+; \delta)}{dx^+} = \frac{d\mathcal{R}^-(x; \delta)}{dx} \Big|_{x=0} = \frac{2}{\delta}.
 \end{aligned}$$

Therefore, it is proven that  $\mathcal{R}^-(x; \delta)$  is differentiable at each point, allowing backpropagation to be performed effectively during the optimization process to update model parameters. The derivative function of  $\mathcal{R}^-(x; \delta)$  can be formulated as follows:

$$\frac{d\mathcal{R}^-(x; \delta)}{dx} = \begin{cases} \frac{2}{\delta}, & \text{if } x \geq 0. \\ \frac{2}{\delta^2}x + \frac{2}{\delta}, & \text{if } -\delta \leq x < 0. \\ 0, & \text{if } x < -\delta. \end{cases}$$

**A.2.2 Smoothness.** To prove the smoothness of  $\mathcal{R}^-(x; \delta)$  is equivalent to proving that the derivation function of  $\mathcal{R}^-(x; \delta)$  is continuous. This continuity is essential for ensuring stable gradient changes for efficient optimization and smooth convergence of the model. For the sake of presentation, let  $\mathcal{D}^-(x; \delta) = \frac{d\mathcal{R}^-(x; \delta)}{dx}$ .

Clearly,  $\mathcal{D}^-(x; \delta)$  is continuous on its three segments, thus we only need to verify that it is continuous at the points where  $x = -\delta$  and  $x = 0$ , which is presented as follows:

$$\begin{aligned}\lim_{x^- \rightarrow -\delta} \mathcal{D}^-(x^-; \delta) &= \lim_{x^+ \rightarrow -\delta} \mathcal{D}^-(x^+; \delta) = \mathcal{D}^-(-\delta; \delta) = 0, \\ \lim_{x^- \rightarrow 0} \mathcal{D}^-(x^-; \delta) &= \lim_{x^+ \rightarrow 0} \mathcal{D}^-(x^+; \delta) = \mathcal{D}^-(0; \delta) = \frac{2}{\delta}.\end{aligned}$$

Therefore, it is proven that  $\mathcal{R}^-(x; \delta)$  is smooth, and the derivative function of  $\mathcal{R}^-(x; \delta)$  is continuous at each point.

**A.2.3 Convexity.** First, it is obvious that  $\mathcal{R}^-(x; \delta)$  is convex on its three segments, thus we only need to verify three situations by proving  $t\mathcal{R}^-(x_1; \delta) + (1-t)\mathcal{R}^-(x_2; \delta) - \mathcal{R}^-(tx_1 + (1-t)x_2; \delta) \geq 0$  for the given  $0 \leq t \leq 1$  and  $x_1 < x_2$ .

1) When  $-\delta \leq x_1 < 0 \leq x_2$ , we have:

$$\begin{aligned}&t\mathcal{R}^-(x_1; \delta) + (1-t)\mathcal{R}^-(x_2; \delta) \\ &= t \left( \frac{1}{\delta^2}x_1^2 + \frac{2}{\delta}x_1 + 1 \right) + (1-t) \left( \frac{2}{\delta}x_2 + 1 \right).\end{aligned}$$

If  $tx_1 + (1-t)x_2 \geq 0$  then:

$$\begin{aligned}\mathcal{R}^-(tx_1 + (1-t)x_2; \delta) &= \frac{2}{\delta} [tx_1 + (1-t)x_2] + 1. \\ t\mathcal{R}^-(x_1; \delta) + (1-t)\mathcal{R}^-(x_2; \delta) - \mathcal{R}^-(tx_1 + (1-t)x_2; \delta) \\ &= \frac{t}{\delta^2}x_1^2 \\ &> 0.\end{aligned}$$

If  $-\delta \leq tx_1 + (1-t)x_2 < 0$  then:

$$\begin{aligned}\mathcal{R}^-(tx_1 + (1-t)x_2; \delta) &= \left\{ \frac{1}{\delta} [tx_1 + (1-t)x_2] + 1 \right\}^2. \\ t\mathcal{R}^-(x_1; \delta) + (1-t)\mathcal{R}^-(x_2; \delta) - \mathcal{R}^-(tx_1 + (1-t)x_2; \delta) \\ &= \frac{t}{\delta^2}x_1^2 - \frac{1}{\delta^2} [tx_1 + (1-t)x_2]^2 \\ &= \left[ \frac{\sqrt{t}}{\delta}x_1 - \frac{t}{\delta}x_1 - \frac{1-t}{\delta}x_2 \right] \left[ \frac{\sqrt{t}}{\delta}x_1 + \frac{t}{\delta}x_1 + \frac{1-t}{\delta}x_2 \right] \\ &> \left[ \frac{\sqrt{t}}{\delta}x_1 - \frac{1}{\delta}x_2 \right] \left[ \frac{\sqrt{t}}{\delta}x_1 + \frac{1}{\delta}x_1 \right] \\ &> 0.\end{aligned}$$

For the other two situations, *i.e.*,  $x_1 < -\delta < 0 \leq x_2$  and  $x_1 < -\delta \leq x_2 < 0$ , the proof process is similar to the situation discussed above, and is therefore omitted for brevity.

In summary,  $\mathcal{R}^-(x; \delta)$  is convex at each point, which facilitates finding the optimal solution while maintaining good convergence speed and stability.

**A.2.4 Non-strictly Monotonically Increasing.** First, it is obvious that  $\mathcal{R}^-(x; \delta)$  is non-strictly monotonically increasing on its three segments, thus we only need to verify the following three situations:

1) When  $-\delta \leq x < 0$ , for given  $\varepsilon > 0$ , if  $x + \varepsilon \geq 0$  we have:

$$\begin{aligned}&\mathcal{R}^-(x + \varepsilon; \delta) - \mathcal{R}^-(x; \delta) \\ &= \frac{2}{\delta}(x + \varepsilon) + 1 - \left( \frac{1}{\delta^2}x^2 + \frac{2}{\delta}x + 1 \right) \\ &= \frac{1}{\delta} \left( 2\varepsilon - \frac{1}{\delta}x^2 \right) \\ &\geq \frac{1}{\delta} \left( -2x + \frac{1}{x} \cdot x^2 \right) \\ &> 0.\end{aligned}$$

2) When  $x < -\delta$ , for given  $\varepsilon > 0$ , if  $-\delta \leq x + \varepsilon < 0$  we have:

$$\begin{aligned}&\mathcal{R}^-(x + \varepsilon; \delta) - \mathcal{R}^-(x; \delta) \\ &= \frac{1}{\delta^2}(x + \varepsilon)^2 + \frac{2}{\delta}(x + \varepsilon) + 1 \\ &= \left[ \frac{1}{\delta}(x + \varepsilon) \right]^2 \\ &> 0.\end{aligned}$$

3) When  $x < -\delta$ , for given  $\varepsilon > 0$ , if  $x + \varepsilon \geq 0$  we have:

$$\mathcal{R}^-(x + \varepsilon; \delta) - \mathcal{R}^-(x; \delta) = \frac{2}{\delta}(x + \varepsilon) + 1 > 0.$$

In summary,  $\mathcal{R}^-(x; \delta)$  is non-strictly monotonically increasing, which can also be supported by the fig. 4c in the main paper.

**A.2.5 Upper Bound of Heaviside Function.** Here we prove  $\mathcal{R}^-(x; \delta)$  is the upper bound of  $\mathcal{H}(x)$ , which is equivalent to prove the  $\mathcal{R}^-(x; \delta) - \mathcal{H}(x) \geq 0$ . Let  $\mathcal{P}^-(x; \delta) = \mathcal{R}^-(x; \delta) - \mathcal{H}(x)$ , we have:

$$\mathcal{P}^-(x; \delta) = \begin{cases} \frac{2}{\delta}x, & \text{if } x \geq 0. \\ \frac{1}{\delta^2}x^2 + \frac{2}{\delta}x + 1, & \text{if } -\delta \leq x < 0. \\ 0, & \text{if } x < -\delta. \end{cases}$$

Obviously,  $\mathcal{P}^-(x; \delta) \geq 0$ , which illustrates the  $\mathcal{R}^-(x; \delta)$  is the upper bound of  $\mathcal{H}(x)$ .

### A.3 Description of the Basic Loss

As outlined in Section 3.4, following previous methods on ranking optimization [13, 52], we combine the AP losses with a basic loss  $\mathcal{L}_{base}$ , which comprises the InfoNCE loss [41] and an SSHN loss [33].

The InfoNCE loss is widely used in self-supervised contrastive learning tasks due to its effectiveness and adaptability. For a query video  $V_k$ , the InfoNCE loss is calculated by:

$$\mathcal{L}_{NCE}^k = -\frac{1}{|S^{k+}|} \sum_{s_{ki} \in S^{k+}} \log \frac{\exp(s_{ki}/\tau)}{\exp(s_{ki}/\tau) + \sum_{s_{kj} \in S^{k-}} \exp(s_{kj}/\tau)}.$$

Using the InfoNCE enables the model to support representation learning by distinguishing between positive and negative instances, thus promoting collaborative optimization between ranking and representation learning.

The SSHN loss promotes self-similarity towards 1 by compensating for the CNN block  $\psi$ , which tends to make  $s_{kk}$  less than 1. Additionally, it performs hard negative mining by reducing the similarity of the most challenging negative instances, thus enhancing the distinction between similarities. The SSHN loss can be formulated as follows:

$$\mathcal{L}_{SSHN}^k = -\log(s_{kk}) - \log \left( \max_{s_{ki} \in S^{k-}} (1 - s_{ki}) \right).$$

Finally, we integrate these two losses as the following basic loss function, where  $\lambda_s$  is hyperparameters to adjust the weights of the two losses.

$$\mathcal{L}_{base} = \frac{1}{N} \sum_{k=1}^N \left( \mathcal{L}_{NCE}^k + \lambda_s \mathcal{L}_{SSHN}^k \right). \quad (16)$$

## A.4 Hierarchical Average Precision Optimization Algorithm

Algorithm 1 outlines the process of our proposed hierarchical AP optimization method.

---

### Algorithm 1 Hierarchical Average Precision Optimization

---

**Input:** Training set  $S$ , maximum iterations  $L$ , learning rate  $\{\eta_l\}_{l=1}^L$ , positive frame rate  $r_t$ , negative frame rate  $r_b$ .

**Output:** Model parameters  $\Theta_{L+1}$ .

- 1: Initialize model parameters  $\Theta_1$ .
  - 2: **for**  $l = 1$  to  $L$  **do**
  - 3:   Sample a batch of videos  $\{V_i\}_{i=1}^N$  from  $S$ .
  - 4:   Extract video embeddings  $g(V_i)$  and  $g'(V_i)$ .
  - 5:   Generate pseudo labels  $\hat{Y}$  based on  $r_t$  and  $r_b$ .
  - 6:   Calculate similarities with function  $f$  in Eq. (5).
  - 7:   Compute  $\widehat{AP}_k^{\downarrow}(f)$  with Eq. (11) to form  $\mathcal{L}_{QLAP}^V$  and  $\mathcal{L}_{QLAP}^F$ .
  - 8:   Compute the total loss  $\mathcal{L}$  by Eq. (15).
  - 9:   Update parameters:  $\Theta_{l+1} = \Theta_l - \eta_l \nabla \mathcal{L}$ .
  - 10: **end for**
- 

## B DETAILED DESCRIPTION OF EXPERIMENTS

### B.1 Datasets

The detailed description of the datasets used in our experiments is as follows:

- **VCDB** [28] is designed for the task of partial video copy detection. It contains a labeled core dataset denoted as VCDB (C) and a large-scale unlabeled dataset with 100,000 distractor videos denoted as VCDB (D). In our experiments, we only use the VCDB (D) for self-supervised training.
- **EVVE** [48] is used as a benchmark video dataset for the task of event-based video retrieval. It includes 620 query videos and 2,373 database videos manually annotated into 13 event categories. Due to the absence of some videos, only 504 query videos and 1,906 database videos can be obtained.
- **SVD** [27] is designed for the task of near-duplicate video retrieval, containing 1,206 queries and 526,787 unlabelled videos in total. The dataset is organized into a training set and a test set. For evaluation in the experiments, we exclusively employ the test set, which includes 206 queries with 6,355 labeled video pairs and 526,787 unlabelled videos as distractors.
- **FIVR-200K** [29] is specifically designed for fine-grained incident video retrieval, comprising 100 queries and 225,960 database videos. It contains three distinct video retrieval subtasks: Duplicate Scene Video Retrieval (DSVR), Complementary Scene Video Retrieval (CSVR), and Incident Scene Video Retrieval (ISVR). Additionally, it also contains three distinct video detection subtasks: Duplicate Scene Video Detection (DSVD), Complementary Scene Video Detection (CSVD), and Incident Scene Video Detection (ISVD).
- **FIVR-5K** [33], a subset of FIVR-200K, which includes 50 queries and 5,000 database videos, containing the same subtasks as FIVR-200K. This dataset is also utilized in our experiments to facilitate swift comparative analysis.

Generally, we use the origin videos from VCDB ( $\mathcal{D}$ ) to train our model and conduct evaluation on EVVE, SVD, FIVR-200K as well as FIVR-5K. Following the previous works [33], we use the extracted features of the evaluation datasets in our experiments. A summary of the descriptions for these datasets is presented in Table 5.

### B.2 Evaluation Metrics

**Mean Average Precision** Mean Average Precision (**mAP**), also known as macro Average Precision [43], serves as the primary metric to evaluate the overall performance of retrieval tasks. Specifically, AP computes the average ranking of positive instances in the retrieval set for a particular query, while mAP calculates the mean of these AP values across all queries. The definition of mAP is given in Eq. (17), where  $n_j$  denotes the number of positive instances for a particular query,  $r_i$  represents the ranking of the  $i$ -th retrieved positive instance in the retrieval set, and  $|Q|$  is the number of query instances.

$$mAP = \frac{1}{|Q|} \sum_{j=1}^{|Q|} \frac{1}{n_j} \sum_{i=1}^{n_j} \frac{i}{r_i} \quad (17)$$

**Micro Average Precision** Micro Average Precision ( **$\mu$ AP**) is a metric employed in prior research [33, 35, 44] to evaluate the performance of detection tasks. In contrast to mAP,  $\mu$ AP considers the joint distribution of similarities across all queries by calculating the AP across all queries simultaneously, which reflects the model's capability to consistently apply a uniform threshold across various queries to detect relevant instances.  $\mu$ AP is computed as outlined in Eq. (18), where  $|R|$  is the number of all reference instances,  $p(i)$  represents the precision of  $i$ -th instance and  $\Delta r(i)$  denotes the difference of recall between  $i$ -th and its adjacent instance in the sorted list according to similarity scores.

$$\mu AP = \sum_{i=1}^{|R|} p(i) \Delta r(i) \quad (18)$$

### B.3 Implementation Details

In this subsection, we provide additional descriptions of implementation details including the data processing, experiment configuration, and hyperparameter settings.

**Data processing** We adopt a self-supervised learning approach as introduced in [33], where videos in a batch are subjected to weak and strong augmentations to simulate common video copy transformations in actual situations. The weak augmentation function set  $\mathbf{A}_w$  includes traditional geometric transformations such as random cropping and horizontal flipping, applied to the frames of the entire video. The strong augmentation function set  $\mathbf{A}_s$ , on the other hand, involves more complex transformations: **1) Global transformations** apply different geometric and optical image transformations on all frames consistently by RandAugment [12]; **2) Frame transformations** encompass overlaying emojis and text on randomly selected frames and applying blur to frames [44]; **3) Temporal transformations**, including fast forward, slow motion, reverse play, frame pause, and sub-clip shuffle/dropout [30, 33], are utilized to create intense temporal manipulations; **4) Video mix-up transformation**, down-scales a video and embeds it within another video [33].

**Table 5: Summary of the descriptions for the VCDB, EVVE, SVD, FIVR-200K, and FIVR-5K datasets.**

Dataset	Video Task	# of Query Videos	# of Database Videos
VCDB	Partial Video Copy Detection	528	100,000
EVVE	Event-based Video Retrieval	620	2,373
SVD	Near-duplicate Video Retrieval	206	526,787
FIVR-200K DSVR / DSVD	Duplicate Scene Video Retrieval / Detection	200	225,960
FIVR-200K CSVN / CSVD	Complementary Scene Video Retrieval / Detection	200	225,960
FIVR-200K ISVR / ISVD	Incident Scene Video Retrieval / Detection	200	225,960
FIVR-5K DSVR / DSVD	Duplicate Scene Video Retrieval / Detection	50	5,000
FIVR-5K CSVN / CSVD	Complementary Scene Video Retrieval / Detection	50	5,000
FIVR-5K ISVR / ISVD	Incident Scene Video Retrieval / Detection	50	5,000

**Experiment configuration** For the training video data, following the previous work [30, 34, 53], we first extract one frame per second for each video. Subsequently, we resize the frames to 256 pixels and crop them to 224 pixels, then randomly select 28 consecutive frames to constitute a video clip. For the backbone feature extractor  $g(\cdot)$ , following previous literature [30, 33, 34], we adopt ResNet50 [22] pretrained on ImageNet [14]. The backbone feature extractor  $g(\cdot)$  performs the mapping  $g : \mathbb{R}^{T \times H \times W \times C} \rightarrow \mathbb{R}^{T \times R \times D}$ , where  $T = 28, H = 224, W = 224, C = 3, R = 9, D = 512$ . For the feature extractor  $g'(\cdot)$  in the pseudo label generator, we utilize DINO [8] pretrained ViT-small [15] with a patch size of 16. The feature extractor  $g'(\cdot)$  performs the mapping  $g' : \mathbb{R}^{T \times H \times W \times C} \rightarrow \mathbb{R}^{T \times D'}$ , where  $T = 28, H = 224, W = 224, C = 3, D' = 384$ .

**Hyperparameter settings** Our model is trained for 30,000 iterations with a batch size of 64. We use AdamW [39] with the Cosine Annealing scheduler for parameters optimization. The learning rate is set to  $4 \times 10^{-5}$  with a warm-up period [38] of 1,000 iterations, and weight decay is set to  $1 \times 10^{-2}$ . For the hyperparameters concerning QuadLinear-AP, we choose  $\delta_v = 0.05, \rho_v = 0.10$  for  $\mathcal{L}_{QLAP}^V$ , and  $\delta_f = 0.05, \rho_f = 5.00$  for  $\mathcal{L}_{QLAP}^F$ . The weights of  $\mathcal{L}_{QLAP}^V$  and  $\mathcal{L}_{QLAP}^F$  are selected as  $\lambda_v = 4$  and  $\lambda_f = 6$ . The top and bottom rates for dividing positive and negative frame instances in the pseudo label generator are set to  $r_t = 0.35$  and  $r_b = 0.35$ . The top-k rates of TopK-Chamfer Similarity within spacial and temporal correlation aggregation are set to  $k_s = 0.10$  and  $k_t = 0.03$ , respectively.

Generally, the settings and hyperparameters for our HAP-VR framework within the training process are summarized in Table 6. All experiments in this work are conducted with Pytorch [42] library on a Linux machine equipped with an Intel Gold 6230R CPU and two NVIDIA 3090 GPUs.

## B.4 Additional Ablation Study

In this section, we explore the impact of hyperparameters in our framework on performance. Except for the specific hyperparameters being investigated, we maintain consistency in all other experimental settings to ensure a fair comparison.

**Impact of  $\delta_v$  and  $\delta_f$**  The results of our model trained with different  $\delta_v$  and  $\delta_f$  are presented in Table 7 and Table 8, respectively. The performance decreases for both hyperparameters when set above or below 0.05. This highlights the importance of selecting the appropriate  $\delta_v$  and  $\delta_f$  values to effectively balance the margin

**Table 6: The settings and hyperparameters for our HAP-VR framework within the training process.**

Hyperparameter	Notation	Value
Training process		
Iterations	/	30,000
Warm-up iterations	/	1,000
Batch size	/	64
Learning rate	/	$4 \times 10^{-5}$
Optimizer	/	AdamW
Learning rate scheduler	/	Cosine
Weight decay	/	$1 \times 10^{-2}$
Backbone feature extractor		
# of frames in a clip	$T$	28
Frame size	$H, W$	224
# of ResNet50 feature patch	$R$	9
# of ResNet50 feature dim.	$D$	512
Pseudo label generator		
# of frames in a clip	$T$	28
Frame size	$H, W$	224
# of ViT-small feature dim.	$D'$	384
ViT-small patch size	/	16
Top frame rate	$r_t$	0.35
Bottom frame rate	$r_b$	0.35
QuadLinear-AP		
Video-level Pos-neg margin	$\delta_v$	0.05
Video-level Pos-pos weight	$\rho_v$	0.10
Video-level AP loss weight	$\lambda_v$	4.00
Frame-level Pos-neg margin	$\delta_f$	0.05
Frame-level Pos-pos weight	$\rho_f$	5.00
Frame-level AP loss weight	$\lambda_f$	6.00
TopK-Chamfer Similarity		
Spacial top-k rate	$k_s$	0.10
Temporal top-k rate	$k_t$	0.03

for correctly ranked positive-negative pairs and the penalty for incorrectly ranked positive-negative pairs.

**Impact of  $\rho_v$  and  $\rho_f$**  The results of our model trained with different  $\rho_v$  and  $\rho_f$  are shown in Table 9 and Table 10, respectively. For  $\mathcal{L}_{QLAP}^V$ , setting  $\rho_v$  as a small value such as 0.2 provides optimal benefits as it more effectively adjusts the weight of positive-positive pairs and thus achieves a trade-off with positive-negative pairs. For  $\mathcal{L}_{QLAP}^F$ , which deals with more ambiguous inter-frame correlations, tuning  $\rho_f$  within the range of 0.2 to 5 allows the model to better adapt to the varying instance distributions across different subtasks.

**Impact of  $\lambda_v$  and  $\lambda_f$**  In Table 11, we report the results of our model trained with various values of  $\lambda_f$  while keeping  $\lambda_v$  fixed at 4 to simplify the comparative analysis. It can be observed that increasing  $\lambda_f$  beyond  $\lambda_v$  leads to an obvious performance gain. This is expected as more challenging frame-level similarities require greater weight for effective optimization. Furthermore, finding a balance between  $\lambda_f$  and  $\lambda_v$  with the weight of  $\mathcal{L}_{base}$  can jointly promote ranking and representation learning, thereby enhancing the overall performance of the model.

**Impact of  $r_t$  and  $r_b$**  In Table 12, we report the results of our model trained with various combinations of  $r_t$  and  $r_b$ . When  $r_t$  and  $r_b$  are equal, setting higher values leads to similar frames being forcibly divided as positive and negative instances, thereby decreasing the model’s discriminating ability. Conversely, setting lower values may cause the model to focus only on easier instances, thus resulting in insufficient learning and optimization. When  $r_t$  and  $r_b$  are different, the performance tends to decrease due to the uneven distribution of positive and negative instances increasing the complexity of similarity learning.

**Table 7: Results on FIVR-5K in video retrieval and detection tasks with mAP (%) and  $\mu$ AP (%) for  $\delta_v$  within  $\mathcal{L}_{QLAP}^V$ . The first and second best results are marked with bold and underline.**

$\delta_v$	Retrieval			Detection		
	DSVR	CSVR	ISVR	DSVD	CSVD	ISVD
0.01	87.32	86.66	80.27	73.53	72.15	63.58
0.05	<b>88.86</b>	<b>87.79</b>	80.34	<b>78.15</b>	<b>76.29</b>	<b>65.88</b>
0.10	<u>88.52</u>	<u>87.38</u>	<u>80.37</u>	<u>76.94</u>	<u>75.40</u>	<u>65.60</u>
0.15	87.34	86.62	<b>80.42</b>	73.27	72.37	64.11

**Table 8: Results on FIVR-5K in video retrieval and detection tasks with mAP (%) and  $\mu$ AP (%) for  $\delta_f$  within  $\mathcal{L}_{QLAP}^F$ . The first and second best results are marked with bold and underline.**

$\delta_f$	Retrieval			Detection		
	DSVR	CSVR	ISVR	DSVD	CSVD	ISVD
0.01	<u>90.30</u>	<b>89.19</b>	<b>81.52</b>	81.17	78.37	<b>69.98</b>
0.05	<b>90.37</b>	<u>89.11</u>	<u>80.94</u>	<b>83.62</b>	<b>80.47</b>	<u>69.30</u>
0.10	89.85	88.52	79.93	<u>82.29</u>	<u>79.57</u>	67.15
0.15	89.55	88.05	79.37	<u>82.29</u>	79.40	65.78

**Table 9: Results on FIVR-5K in video retrieval and detection tasks with mAP (%) and  $\mu$ AP (%) for  $\rho_v$  within  $\mathcal{L}_{QLAP}^V$ . The first and second best results are marked with bold and underline.**

$\rho_v$	Retrieval			Detection		
	DSVR	CSVR	ISVR	DSVD	CSVD	ISVD
0.02	89.52	88.45	80.84	78.34	76.39	65.98
0.2	<b>90.28</b>	<b>89.10</b>	<b>81.09</b>	<b>81.39</b>	<b>78.64</b>	<u>68.79</u>
1.0	<u>89.89</u>	<u>88.81</u>	<u>81.03</u>	<u>80.41</u>	<b>78.64</b>	<b>69.41</b>
5.0	89.51	88.31	80.77	80.00	<u>77.59</u>	67.20
50	89.37	88.16	80.89	79.92	77.19	66.91

**Table 10: Results on FIVR-5K in video retrieval and detection tasks with mAP (%) and  $\mu$ AP (%) for  $\rho_f$  within  $\mathcal{L}_{QLAP}^F$ . The first and second best results are marked with bold and underline.**

$\rho_f$	Retrieval			Detection		
	DSVR	CSVR	ISVR	DSVD	CSVD	ISVD
0.02	89.71	88.01	79.44	82.73	78.98	65.80
0.2	<u>90.21</u>	89.01	80.92	<b>83.81</b>	<b>80.59</b>	69.13
1.0	<b>90.37</b>	<b>89.11</b>	80.94	<u>83.62</u>	<u>80.47</u>	69.30
5.0	90.17	<u>89.07</u>	<b>81.29</b>	82.93	80.18	<b>70.99</b>
50	88.77	87.74	<u>81.18</u>	79.76	78.46	<u>70.73</u>

**Table 11: Results on FIVR-5K in video retrieval and detection tasks with mAP (%) and  $\mu$ AP (%) for the weight of  $\mathcal{L}_{QLAP}^F$ , i.e.,  $\lambda_f$ . The first and second best results are marked with bold and underline.**

$\lambda_f$	Retrieval			Detection		
	DSVR	CSVR	ISVR	DSVD	CSVD	ISVD
2	89.73	88.50	80.42	80.45	77.89	66.32
4	<u>90.21</u>	<u>89.08</u>	<u>81.33</u>	<u>83.15</u>	<u>80.69</u>	<u>70.61</u>
6	<b>90.26</b>	<b>89.18</b>	<b>81.47</b>	83.05	80.11	70.32
8	90.07	88.91	81.30	<b>84.20</b>	<b>80.97</b>	<b>70.63</b>

**Table 12: Results on FIVR-5K in video retrieval and detection tasks with mAP (%) and  $\mu$ AP (%) for  $r_t$  and  $r_b$ . The first and second best results are marked with bold and underline.**

$r_t$	$r_b$	Retrieval			Detection		
		DSVR	CSVR	ISVR	DSVD	CSVD	ISVD
0.30	0.30	<u>90.17</u>	88.92	80.90	<u>83.08</u>	80.10	69.02
0.35	0.35	<b>90.21</b>	<b>89.08</b>	<b>81.33</b>	<b>83.15</b>	<b>80.69</b>	<u>70.61</u>
0.40	0.40	<u>90.17</u>	<u>89.07</u>	<u>81.29</u>	82.93	<u>80.18</u>	<b>70.99</b>
0.45	0.45	89.63	88.37	80.89	82.28	79.38	70.18
0.30	0.40	89.73	88.62	81.18	82.67	79.68	69.18
0.40	0.30	89.82	88.58	80.62	82.28	79.33	69.18

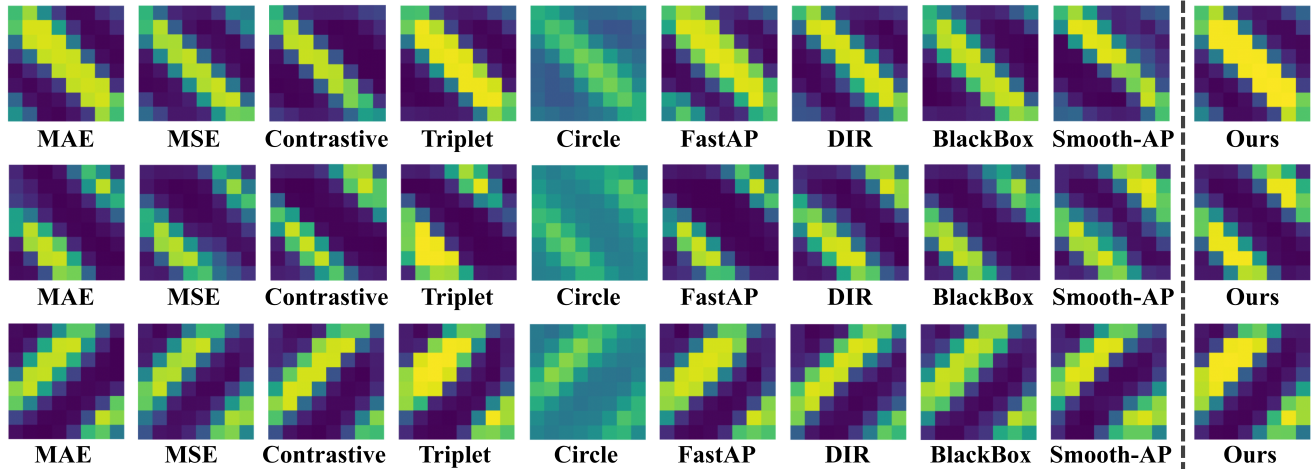


Figure 7: Heatmaps of frame-level similarity matrices generated by various losses. In contrast, our QuadLinear-AP distinguishes between relevant and irrelevant instances more clearly. A brighter color indicates a higher similarity score.

## C VISUALIZATION

In this section, we provide examples to compare frame-level similarity matrices under different losses through visualization for intuitive analysis. The experiment settings remain consistent with those described in Section 4.3 of the main paper. By analyzing these heatmaps, we can make the following observations:

1) Circle loss struggles to distinguish instances clearly even after parameter adjustments, likely due to its sensitivity of data distribution making it perform poorly in challenging video data with an

imbalanced distribution. 2) Triplet loss is prone to become overconfident, which may lead to more irrelevant instances being predicted as relevant, thus increasing the risk of overfitting. 3) While other loss functions can discriminate between instances, there is still room for improvement in their performance. 4) Compared to other competitors, our proposed QuadLinear-AP generates higher similarity scores for relevant pairs of frames while lower scores for the irrelevant ones, thereby creating a clearer fine-grained distinction between the pairs compared to other competitors. provides a clearer distinction between relevant and irrelevant instances, making it effective for video retrieval tasks.